

1994

Reaction of Ti, Ti/Ni and Ti/Pt thin films on AlN substrates

Yoshihiko Imanaka
Lehigh University

Follow this and additional works at: <http://preserve.lehigh.edu/etd>

Recommended Citation

Imanaka, Yoshihiko, "Reaction of Ti, Ti/Ni and Ti/Pt thin films on AlN substrates" (1994). *Theses and Dissertations*. Paper 272.

This Thesis is brought to you for free and open access by Lehigh Preserve. It has been accepted for inclusion in Theses and Dissertations by an authorized administrator of Lehigh Preserve. For more information, please contact preserve@lehigh.edu.

AUTHOR:

Imanaka, Yoshihiko

TITLE:

**Reaction of Ti/Ni and Ti/Pt
Thin Films on AlN
Substrates**

DATE: May 29, 1994

**Reaction of Ti, Ti/Ni and Ti/Pt Thin Films
on AlN Substrates**

by

Yoshihiko Imanaka

A Thesis

Presented to the Graduate Committee

of Lehigh University

in Candidacy for the Degree of

Master of Science

in

Materials Science and Engineering

Lehigh University

1994

Certificate of Approval

This thesis is accepted and approved in partial fulfillment of the requirements for the degree of Master of Science.

May 18, 1994

Date

Professor in Charge

Chairman of Department

Acknowledgment

I wish firstly to acknowledge the support, guidance and constant encouragement of my adviser Professor Michael R. Notis who helped me personally, academically and socially. He listened to me very patiently and spoke to me very clearly and carefully while selecting words I can understand. Because he understands Japanese culture and Japanese people's behavior very well, he warmly and sincerely accepted my very Japanese way which American people sometimes don't understand. I very much appreciate his discipline for making me grow into one of the Japanese people with an international view, and who can survive in the world (But, I'm not sure if I meet his expectation.).

I also would like to thank the Department of Material Science & Engineering. The hard curriculum made me keep busy. Since my characteristics seems to be neglect, I couldn't have learned a lot of things in the United States, if it were easy. I can't forget the kind cooperation and warm support of all of the staff in Material Science & Engineering. Even if I acknowledge them over and over again, it could not be exaggerated.

Surely, I wish to acknowledge my wife, Yoko. She supported and encouraged me in an unusual way. I sometimes got upset at that way, but as I got used to it, I understood that is a different and helpful affection. My work wouldn't have been done if my parents, Eizaburo and Atsuko didn't help me in a warm manner. They always encouraged me to keep a positive attitude. Finally, I wish to sincerely acknowledge our company, Fujitsu Laboratories Ltd. for giving me this great opportunity, and which I might not be able to have ever accomplished without their commitment to me.

Table of Contents

	Page #
Certificate of Approval	ii
Acknowledgements	iii
Table of Contents	iv
List of Tables	v
List of Figure Captions	vi
1. Abstract	1
2. Introduction	2
3. Background	4
3.2 Aluminum nitride substrate in microelectronic packaging	15
3.3 Thin film metallization of AlN	21
3.4 Reaction between AlN and Ti	25
3.5 Rutherford backscattering spectrometry (RBS)	32
4. Materials and Experimental Procedures	37
5. Results and Discussion	40
5.1 Reaction between Ti thin film/AlN substrate	40
5.2 Reaction between Ni/Ti/AlN substrate	56
5.3 Reaction between Pt/Ti/AlN substrate	66
6. Conclusion	73
7. References	75
8. Vita	82

List of Tables

	page #
Table 1 Property comparisons between AlN and Al ₂ O ₃ .	13
Table 2 Properties of typical conductors used in microelectronics.	14
Table 3 Properties of heat sink candidate materials.	18
Table 4 Pull test adhesion studies of thin film film metallization on AlN.	19
Table 5 Reaction studies between AlN and Ti.	24
Table 6 Rapid thermal annealing conditions used in this study.	39

List of Figure Captions

	page #
Figure 1 Growth in level of integration.	5
Figure 2 Input-output terminals vs. electronic content.	6
Figure 3 Chip-pad spacing requirements.	8
Figure 4 Trends in leading edge line pitch.	9
Figure 5 Power density requirements.	11
Figure 6 Phase diagram of Ti-Al-N system at 600°C.	26
Figure 7 Schematic diagram of solid analysis by RBS.	29
Figure 8 Relation between mass ratio and kinematic factor for various backscattering angles.	30
Figure 9 Relation between target mass M_2 and kinematic factor for various ion beams (Backscattering angle, $\theta=170^\circ$).	31
Figure 10 RBS spectrum for a thin metal layer on a silicon substrate.	33

Figure 11	Example comparing the RBS spectra obtained for a gold film on a pure Si substrate (top) to that for Au distributed as a uniform impurity in a bulk alloy (bottom).	34
Figure 12	RBS spectrum for the as-deposited Ti/AlN specimen.	41
Figure 13	RBS spectrum of the as-deposited Ti/AlN specimen deposited by Stanford University.	42
Figure 14	AES depth profile of the as-deposited Ti/AlN specimen from Stanford University.	43
Figure 15	Gibbs free energies of the reactions concerning Ti and AlN, as a function of temperature.	46
Figure 16	Interdiffusion coefficients of Ti-N, TiN and TiAl ₃ obtained from literature data.	47
Figure 17	Interdiffusion coefficients of the Ti-N and Al-Ti reactions from the literature.	52
Figure 18	Comparison of the Arrhenius plots for nitrogen diffusion in α -Ti.	53

Figure 19	RBS spectrum of the as-deposited Ni/Ti/AlN specimen.	54
Figure 20	RBS spectrum for the Ni/Ti/AlN specimen annealed at 600°C for 15 min. in N ₂ atmosphere.	55
Figure 21	RBS spectrum for the Ni/Ti/AlN specimen annealed at 750°C for 15 min. in N ₂ atmosphere.	57
Figure 22	RBS spectrum for the Ni/Ti/AlN specimen annealed at 900°C for 15 min. in N ₂ atmosphere.	58
Figure 23	Schematic diagram of Ni/Ti/AlN diffusion and reaction sequence in N ₂ atmosphere as a function of temperature.	59
Figure 24	Gibbs free energies for reactions involving Ni/Ti/AlN, as a function of temperature.	60
Figure 25	Gibbs free energies for reactions involving Ni/Ti/AlN, and considering the reaction with atmosphere.	61
Figure 26	Arrhenius plot of the interdiffusion coefficient regarding Ni/Ti/AlN reactions.	63
Figure 27	Schematic diagram of the reaction of Ti/AlN annealed in Ar atmosphere.	65

Figure 28 RBS spectrum of the as-deposited Pt/Ti/AlN specimen. 69

Figure 29 RBS spectrum of the Pt/Ti/AlN specimens annealed 70
at 600°C for 15 min. in N₂ atmosphere.

Figure 30 Superimposed RBS spectra of the Pt/Ti/AlN specimens 71
annealed at 750°C and 900°C for 15 min. in N₂
atmosphere.

Figure 31 Schematic diagram of the reaction sequence between 72
Pt/Ti/AlN annealed in a N₂ atmosphere at different
temperatures.

1. Abstract

AlN is a promising material for microelectronic packaging because of its high thermal conductivity and a coefficient of thermal expansion close to silicon. To make use of AlN effectively, the metallization processing of AlN is an essential technology. Thin film metallization permits the fabrication of fine patterns which enables the miniaturization of circuit elements. However, this metallization method must provide high reliability and good adhesion at the interface between AlN and the deposited thin metal film. Because this adhesion is often controlled by heat treatment and interdiffusion, we have studied these effects. Ti films about 0.1-0.15 μm thick were deposited on polished high thermal conductivity AlN surfaces. In most cases these were also overcoated with about the same thickness of Pt or Ni. Specimens were heated in a rapid thermal annealing furnace using N_2 or Ar, for 15 minutes at temperatures ranging from 600°C to 900°C. Interdiffusion and reaction at thin film interfaces were studied using Rutherford Backscattering Spectrometry (RBS). As a result, it is found that Ni/Ti and Pt/Ti reactions are more rapid than Ti/AlN. This result is in good agreement with diffusion data reported in the literature. Therefore, in the case of Ni/Ti/AlN and Pt/Ti/AlN, in order to form interfacial reaction compounds, such as TiAl_3 and TiN , at the interface between Ti/AlN, it appears that a two-step thin film deposition process is required together with an interim heat treatment in order to form interfacial reaction products at the Ti/AlN interface prior to the thin film deposition of Ni or Pt.

2. Introduction

Great progress has been made during the last decade to increase the operational speed of Large Scale Integrated circuits (LSIs). The demand for microelectronic packaging technology to make use of LSIs, has also been increasing. There are two major requirements for this packaging technology.

One is miniaturization of circuits elements. This requirement derives from the demand for faster computers and down-sizing of products. To achieve miniaturization of circuits the circuit line dimensions which connect each LSI element, should be finer and shorter. Nowadays, thick film technology, which limits circuit line widths to greater than 50 μm , has been widely used. Thin film technology makes it possible to reduce the circuit line width below 50 μm . Therefore, the use of thin film technology must be taken into account and incorporated by the packaging designer.

Another requirement is thermal dissipation management. As the performance demands for LSI technology increase, the heat generated can no longer be ignored. One of the methods to dissipate heat effectively is by using a heat sink substrate which has high thermal conductivity.

If the above two packaging requirements are combined together and applied to the next generation in microelectronic packaging, one conception of this design approach is the use of circuit substrates having high thermal conductivity and applying thin film technology directly on the substrate. The substrate should also have high electrical insulating resistance and should provide a thermal expansion match close to silicon.

Matching of thermal expansion allows the minimization of the stress generated between substrate and LSI chip during thermal cycling.

AlN is one of the materials which meet the substrate requirements described above. That is to say, the thermal conductivity is around 200 W/mK in commercial products, and the thermal expansion coefficient is $4.3 \times 10^{-6}/^{\circ}\text{C}$, which is close to the value of the thermal coefficient of expansion of silicon, $3.4 \times 10^{-6}/^{\circ}\text{C}$. Also, AlN possesses a high electrical insulating resistivity of $10^{15} \Omega\cdot\text{cm}$. Therefore, AlN substrates using directly applied thin film technology satisfy the two major requirements for microelectronic packaging.

Thin film metallization of AlN is a key technology. However, this metallization method must provide high reliability and good adhesion between the metal thin film and the AlN substrate. Adhesion is often controlled by heat treatment and interdiffusion. Therefore, an understanding of the reactions and interdiffusion between the metal thin film and AlN is very important and provides an understanding of the direction needed for improving reliability and adhesion strength.

In this study, interdiffusion between metal thin films and AlN, are examined using Rutherford Backscattering Spectrometry (RBS). In consideration of the industrial interest, Ti, Ti/Ni and Ti/Pt thin films, which have been shown to provide high adhesion strength, are used for this study. The following sections therefore review the current directions in microelectronics, the use of AlN as a packaging material, thin film metallization technology for AlN, reactions at Ti/AlN interfaces, and an introduction to the use of RBS for thin film studies.

3. Background

3.1 Current directions in microelectronics

Currently, development and use of Large Scale Integrated circuit (LSI) has been growing at an increasing rate and, accordingly, the demand for microelectronic packaging has been directed at obtaining denser and denser package designs¹⁻³. Figure 1 shows the Dynamic Random Access Memory (DRAM) bits per chip and the number of logic circuits per chip versus time in years. As for DRAM, the number of bits per chip increased exponentially with increasing time. Currently, the development and research of 64M bit chip have proceeded rapidly in semiconductor device manufacturing companies. Logic LSIs (Figure 1) are divided into two types, Complementary Metal-Oxide Semiconductor (CMOS) logic and Bipolar logic; growth of both types also follows an exponential dependence on time. CMOS devices are composed of P-type and N-type Metal-Oxide Semiconductors (MOS) and are used to achieve low power consumption. On the other hand, Bipolar logic devices have the feature that the signal propagation delay time is relatively lower than CMOS logic.

Densifying the number of circuits in a logic chip causes an increase in the number of terminals in the chip. Figure 2 shows the number of input-output (I/O) terminals versus electronic content (Bits per chip). In the case of memory chips, the required number of terminals remains small. For example, a 4 K ($4,096=2^{12}$) bit Random Access Memory (RAM) requires 12 address lines (terminals), and 16 M bit RAM requires 24 address terminals. Control operations such as read, write and clock, require a few

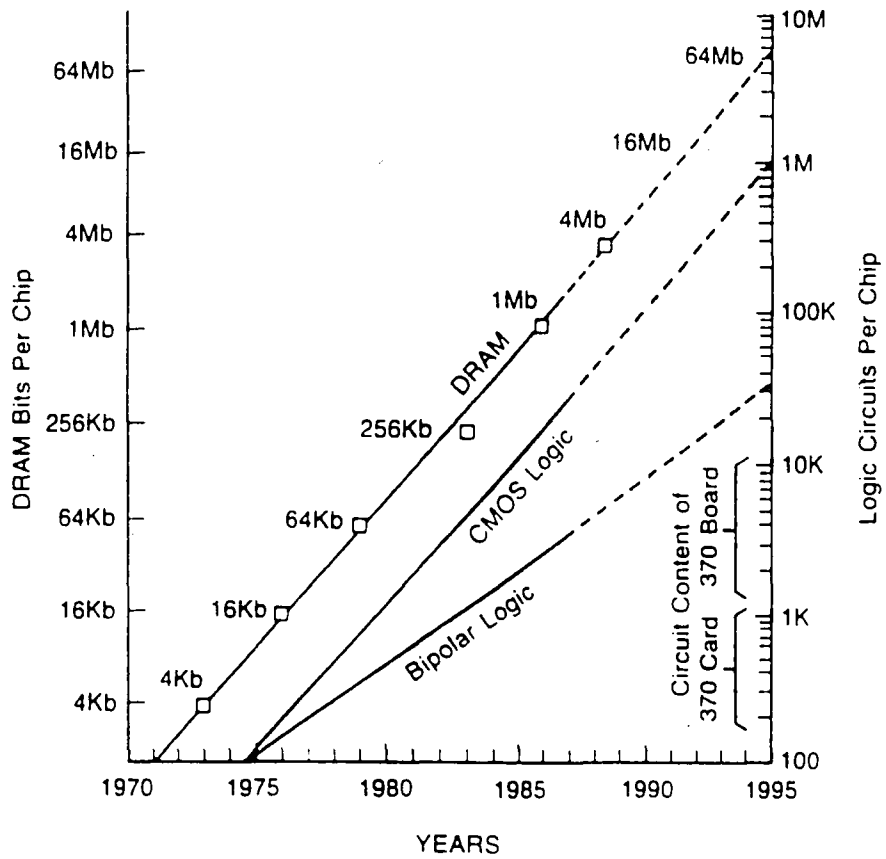


Figure 1 Growth in level of integration [2].

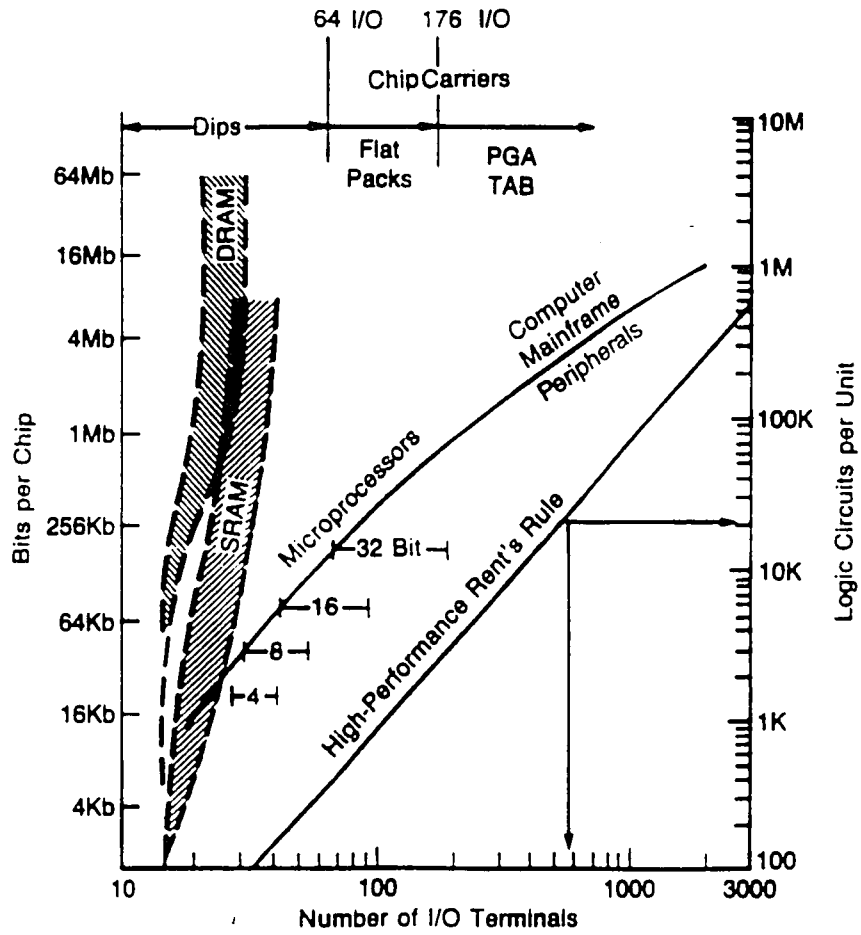


Figure 2 Input-output terminals vs. electronic content [2].

more lines. Thus, the packaging of Memory Devices is usually simple. In contrast, high performance random logic needs a large number of I/O terminals. Usually, the number of terminals in this type of chip follows Rent's law⁴ (Figure 2)

$$ckt = \left(\frac{N}{K} \right)^n,$$

where N: number of signal terminals (pinout).

ckt: average number of circuits supported by N terminals

K: constant. For high-performance applications, $K \cong 2.5$ is used.

n: another constant. For high-performance packaging, in the 10 to 100,000 circuits range, it is said that the best fit is 1.79.

Increasing the number of I/O terminals leads to increasing interconnection density; Figure 3 shows chip pad spacing requirements. Increasing interconnection density means increasing number of chip pads, which are portions of the conductive pattern necessary for connecting to a circuit board. As the number of chip pads is increased, the chip pad spacing must be decreased. Therefore, line width on the circuit board should be decreased. Figure 4 shows trends of leading edge line pitch periodicity. Presently, ceramic circuit boards for which line width is around 80 μm , are used. However, in ceramic circuit boards the smallest achievable line width is currently limited by the nature of thick film technology. It is thought that the limitation is $\sim 50 \mu\text{m}$, because the resolution of the screen mask and the rheology characteristics of the conductive paste limit line width capability. Therefore, circuit board design incorporating thin film technology, which enables the formation of fine line-widths, is desired in most leading-edge microelectronic applications.

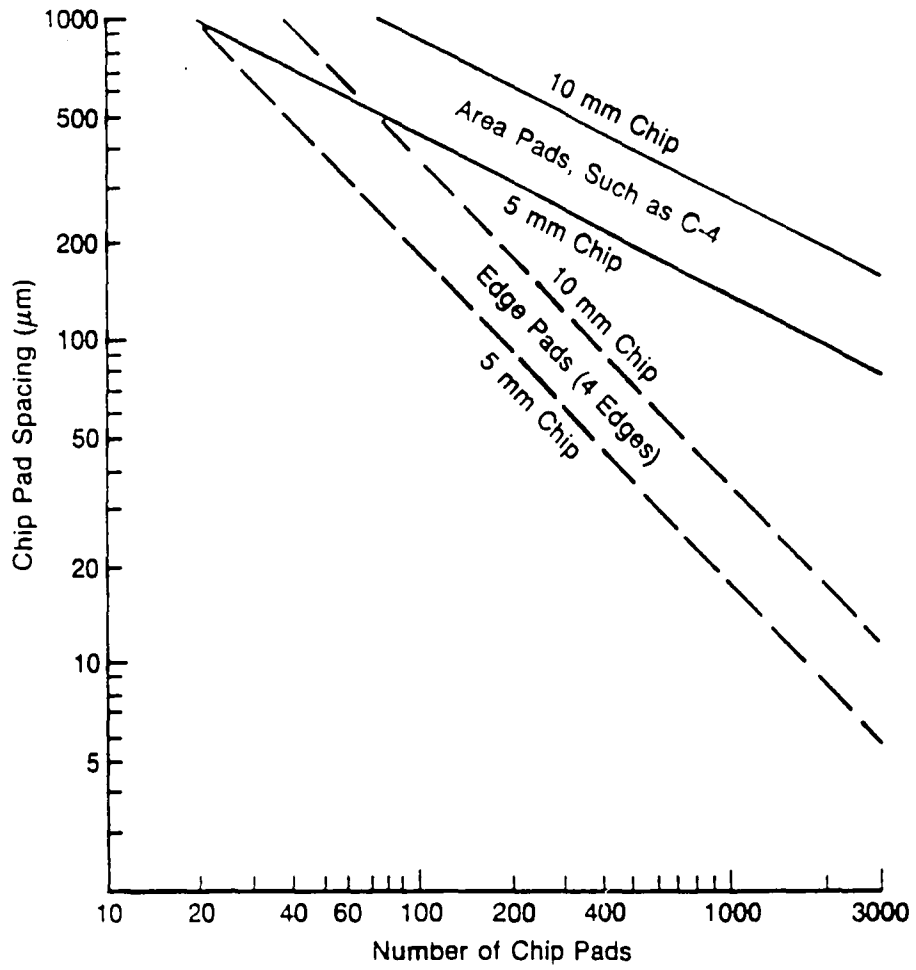


Figure 3 Chip-pad spacing requirements [2].

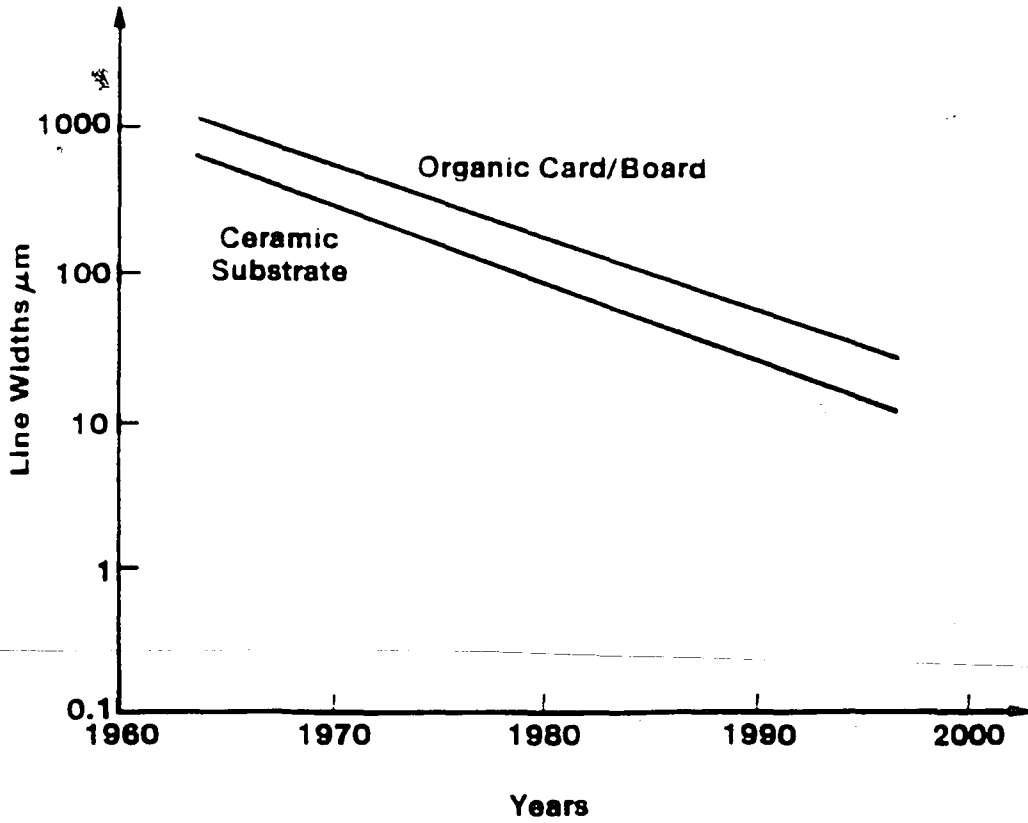


Figure 4 Trends in leading edge line pitch [2].

In this manner, advances in integrated circuit technology causes ever-smaller devices, interconnections and terminals. Following this trend, heat removal becomes a major design issue. Figure 5 shows the power density (W/cm^2) demands of 10 x 10 mm chips with various numbers of circuits and different operating power levels per circuit. It also shows the range of temperature and power densities generated by a light bulb and at the sun's surface. To assure proper electrical performance and limit the propensity to fail, the chip temperature must be maintained below 100°C.

In fact, power densities at the component level have increased dramatically over the years. For example, although a 5 x 5 mm chip dissipating 10 W results in a heat flux of $4 \times 10^5 W/cm^2$ in a mainframe computer, this is not an unusual operating condition. This is only about two orders of magnitude less than that generated on the sun's surface. Yet, the surface temperature of the sun is 6000°C, compared to a maximum operating temperature in the range of 100°C for a typical semiconductor chip.

The thermal dissipation performance of microelectronic packaging is often characterized by its thermal resistance, which is defined as

$$R = \frac{\Delta T}{Q}$$

where, ΔT : temperature drop, °C

Q: heat flow, W

Packaging for relatively low-power systems, such as in personal computers (PCs) and work stations, often have high thermal resistance near 100°C/W. On the other hand, mainframe computers with higher component power dissipation often have a thermal resistance of less than 10°C/W. However, recently the boundary between super-minicomputers

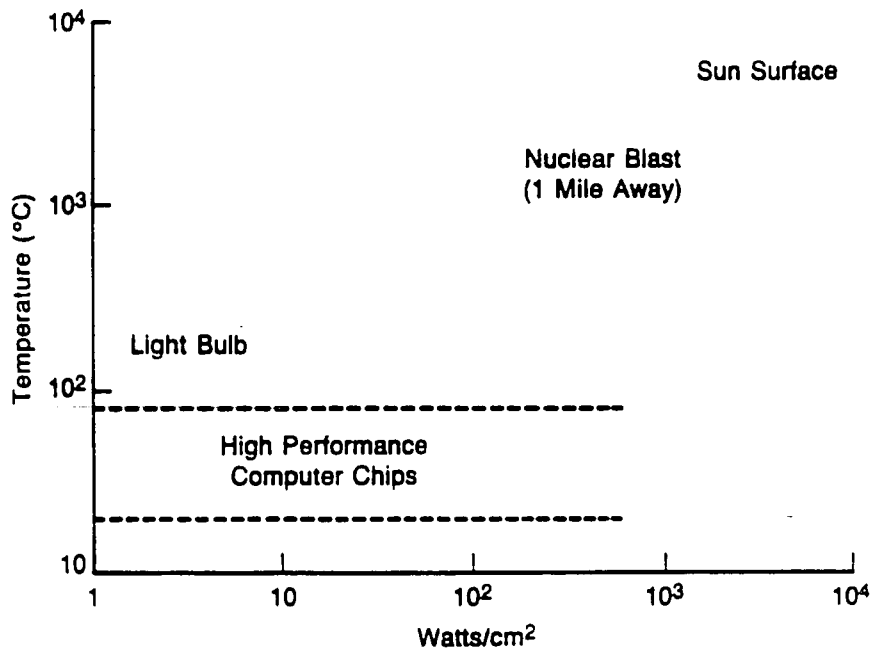
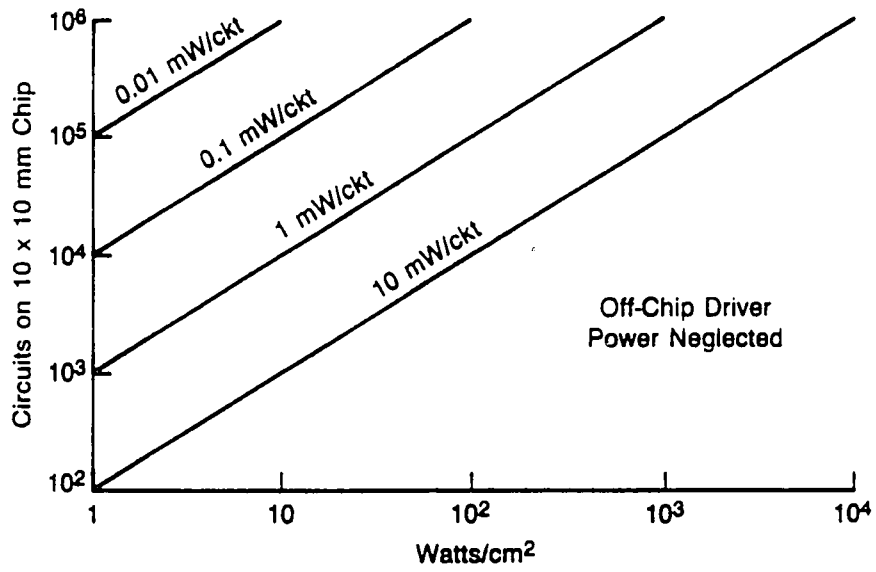


Figure 5 Power density requirements [2].

and mainframe computers is becoming blurred, again, because of progress in LSI technology. In other words, larger capacity PCs now need high performance cooling systems similar to mainframe computers. However, liquid cooling methods and high cost approaches such as Thermal Conduction Modules (TCMs)⁵ used in mainframe computers can't be applied to PCs, because of the large equipment size required for these approaches. For example, in the TCM design of IBM, a spring-loaded aluminum piston in a He atmosphere conducts the heat released by each chip to an Al hat and then to a water-cooled cold plate. That is to say, a TCM requires a water circulation system to keep the plate cold. Therefore, improvement of air cooling such as control of the flow direction of forced-air, and improved design of air entrance, exit and fan location are useful for new PCs. Also, and possibly most dependable, is the use of effective solid heat sinking. Heat sinks are often attached directly to LSI chips to dissipate heat efficiently. If the heat sink is attached using metallization and subsequent metal joining methods, thermal expansion matching to silicon is required for the heat sink material and joint, because the thermal stress generated by the temperature difference between the LSI chip (Si) and heat sink should be minimized. Otherwise, thermal stress causes microcrack formation and leads to high thermal resistance or failure. Another essential requirement for the heat sink material is high thermal conductivity as mentioned previously. Finally, because of the demand for down-sizing and the desire for light-weight products (especially in PCs) low density materials are desirable.

Table 1 Property comparisons between AlN and Al₂O₃.

	AlN	Al ₂ O ₃
Dielectric constant (1 MHz)	9	10
Thermal expansion coefficient (x 10 ⁻⁶ /°C)	4.3	6.7
Insulating resistivity at R.T (Ω•cm)	10 ¹⁵	10 ¹³
Thermal conductivity (W/mK)	230	20
Flexural strength (MPa)	350	300
Sintering temperature (°C)	1800	1600
Cost (arb. unit)	50	1

Table 2 Properties of typical conductors used in microelectronics.

Material	Resistivity ($\mu\Omega\cdot\text{cm}$)	Melting point ($^{\circ}\text{C}$)	
Tungsten (W)	5.5	3387	
Molybdenum (Mo)	5.2	2610	
Aluminum (Al)	2.7	660	Low m. p.
Gold (Au)	2.2	1063	Expensive
Copper (Cu)	1.7	1083	
Silver (Ag)	1.6	961	Migration problem

3.2 Aluminum nitride substrates in microelectronic packaging

Table 1 shows a comparison of the properties of AlN and Alumina (Al_2O_3). When AlN emerged as a possible substrate material for use in microelectronics^{6,7}, Al_2O_3 was widely used for hybrid integrated circuit (IC) technology. However, AlN is considerably better than Al_2O_3 in terms of thermal conductivity. The rest of the properties of AlN are similar to those of Al_2O_3 . Therefore, it is believed that AlN can replace Al_2O_3 for use in hybrid ICs. Yet, as far as present cost is concerned, AlN is 50 times as expensive as Al_2O_3 . The technological merit of a hybrid IC is being able to produce compact circuit structure cheaply and mount ICs densely. Because of the current high cost of AlN, AlN has yet not been applied in mass production of hybrid ICs. However, as development continues and production costs are lowered, consideration of AlN becomes an appealing alternative to Al_2O_3 .

Next, AlN was examined as a candidate material for Multilayer Ceramic Circuit boards (MCC). In conventional systems such as the IBM 3090 TCM, Al_2O_3 was used as the insulating material of the MCC. In MCCs, the insulating material and the conductor are cofired together. The sintering temperature of AlN is slightly higher, but similar to that of Al_2O_3 . Therefore, in consideration of the choice of the conductive material used for co-firing, the same materials used in the Al_2O_3 system, such as Molybdenum (Mo) and Tungsten (W) can also be used with the AlN system.

Basically, the merit of the MCC approach is being able to incorporate high reliability long circuit interconnections in a small space. However, the application of such circuit designs is limited. One useful application of

MCCs is in a mainframe computer, which might require more than 100 LSI chips to form its central processing unit (CPU). Considering packaging design, the length of circuit interconnections should be as short as possible. There are two main reasons why the circuit length should be shortened. Conductive lines possess measurable resistivity which causes signal transmission loss, and a major requirement of a conductive line is, therefore low resistivity. However, even if a material with low resistivity is used in the circuit, the signal can still be attenuated and distorted with increasing length of wiring and with decreasing cross-sectional area of wiring. If the signal is attenuated too much, the signal can't be recognized as a signal pulse. Another problem is related to the signal speed. Physically, if the length of circuit between LSIs is short, the signal speed between LSIs is faster. To make use of high-performance LSIs effectively, short-length circuits are necessary. Otherwise, even if high-speed LSIs are used, the whole circuit may still produce a long propagation delay time. Therefore, even in the mainframe computer, packaging designers make considerable effort to shorten the circuit length. As for the circuit boards of mainframe computers, the MCC approach is reasonable in order to meet the demand of incorporating long circuit structures within a three-dimensional small space.

However, as mentioned above, the conductor should have low resistivity. W which is used for metallization of AlN, can't satisfactorily meet this requirement because it has a relatively high bulk resistivity. Table 2 shows typical conductor materials used in the microelectronics field. This table indicates copper to be one of the best conductors. Although silver has lower resistivity than copper, silver sometimes

generates short-circuits because it is easy to ionize and forms dendrites in an electric field. In fact, copper is the most common metal used in printed circuit board applications. However, because the melting point of copper is 1083°C (low in comparison to the sintering temperature for alumina ceramics), development of the ceramics whose firing temperature is about 1000°C is necessary in order to use copper conductors for MCC. The ceramics of interest for use with copper conductors are glass-ceramics and glass/ceramic composites; they have sintering temperatures in the same range as copper and therefore can be cofired with copper. These materials possess a silica rich glass phase in the microstructure, which leads to a lower dielectric constant. Typically these glassy materials have dielectric constants around six. In contrast, the dielectric constant of AlN is nine. The signal propagation delay time of the wiring adjacent to an insulated material is proportional to the square root of the dielectric constant of the insulating material.

$$Tpd = \frac{\sqrt{\epsilon}}{C}$$

where,

ϵ : relative dielectric constant of the insulating material

C: speed of light (3×10^8 m/sec)

Tpd: signal propagation delay time (ns/m)

That is to say, judging its utility based on dielectric constant, AlN is not a good material in terms of its use in MCC.

In order to make use of AlN most effectively, it therefore appears suitable as substrates on which to form thin film circuits, and for use as a

Table 3 Properties of heat sink candidate materials.

Material	Thermal Conductivity (W/mK)	Thermal Expansion Coefficient ($\times 10^{-6}/^{\circ}\text{C}$)	Density (g/cm^3)
Al	240	23	2.70
Cu	393	17	8.93
Cu-W alloy (20% Cu)	248	7	17.2
AlN	230	4.5	3.30
Al ₂ O ₃	17	7.0	3.98
Diamond (CVD method)	400	2.3	3.52
Diamond (High pressure)	2000	2.3	3.52
Polyimide	0.2	50	1.38
Si		3.4	

Table 4 Pull test adhesion studies of thin film metallization on AlN.

Author	Thin film system	Adhesion strength (kg/mm ²)	Pad size (mm)	Note
Kurokawa et al. (NEC) [14] '85	Ti/Pd/Au	2.5	2 x 2	
	NiCr/Pd/Au	2.5		
	Ta ₂ N/NiCr/Pd/Au	2.5		
Chanchani et al. (AT&T) [15, 16] '88	Ti/Pd/Au	3.95	1.072 x 0.76	
	Ta ₂ N/Ti/Pd/Au	3.95		
Drost et al. '90 (Fraunhofer) [17]	TiW/Au	0.97	2 x 2	
	NiCr/TiW/Au	1.045		
	NiCr/Ni/Au	1.377		
Lodge et al. '90 (Plessey Research Caswell Ltd.) [18]	NiCr/Au	(4.1) arb. unit	unknown	
	Ti/Pt/Au	(6.6)		
Yasumoto et al. (Toshiba) [19] '93	Ti/Ni	4.5	2 x 2	post anneal 830°C- 5 min.
	Zr/Ni	4.5		
	Cr/Ni	4.5		
	Ta/Ni	4.5		
	Ni	0.045		

heat sink material. Both applications focus on the high thermal conductivity and the thermal expansion match close to silicon, the LSI material. Although AlN has a relatively high dielectric constant, if multilayer structures with organic material films having low dielectric constant are used as a thin insulated layer on AlN (which is also an insulating material), the drawback of AlN as a dielectric is ameliorated. Because organic materials have low dielectric constants, but also low thermal conductivity, AlN takes the burden of heat dissipation. In this type of system, thin film wiring can be formed on AlN and in the organic material. Organic materials such as polyimide and benzocyclobutene (BCB), which have a dielectric constant below four, can be formed on AlN using a spin-coat method⁸. Metal thin films can be formed on AlN and on organic layers, using a variety of sputtering methods. By continuing the procedure of depositing organic films and metal films alternately, multilayer circuit structures can be formed. This structure, including the AlN substrate, meets many of the demands for microelectronic packaging described in section 3.1. In this manner the thin film multilayer structures deposited on a substrate take into account the thermal management requirements.

Table 3 shows the typical relevant properties of candidate heat sink materials. Diamond has the best performance in terms of heat sink requirements, but, in terms of current low cost industrial application, it is still an immature technology. As mentioned in section 3.1, the requirements for heat sink materials are not only high thermal conductivity, but also a thermal expansion match close to silicon and low density. AlN meets all of the requirements best when compared with other candidates

shown in Table 3. In fact, most microelectronics companies are currently using AlN in applications where heat sink technology is important⁹⁻¹³. However, to make use of AlN effectively as a thin film substrate and for heat sink applications, the study of high reliability methods for metallization and a knowledge of the mechanisms⁴ to obtain good adhesion are necessary.

3.3 Thin film metallization of AlN

Because AlN was recognized as a good candidate material for hybrid IC and MCC applications, many papers regarding thick film metallization of AlN have been reported. However, reports regarding thin film metallization of AlN have only started to appear relatively recently in the literature. Table 4 lists the adhesion strength (pull test) studies, which have already been published.

Kurokawa et al., at NEC, reported in 1985 that he examined Ti/Pd/Au, NiCr/Pd/Au and Ta₂N/NiCr/Pd/Au thin film systems on AlN¹⁴. They used a conventional sputtering method to form these multilayer films. The adhesion strength of Ti/Pd/Au or NiCr/Pd/Au metallization was 2.5 kg/mm², when the pad size of the metal film was 2 x 2 mm². Although it is not listed in the table, they also reported good adhesion strengths for Ni and Cu, formed by an electroless plating method, which were 2.6 and 2.4 kg/mm², respectively. The adhesion strength of thick film metallization on AlN, such as Ag-Pd and Cu, is reported to be around 2.2 kg/mm². Considering these thick film adhesion strengths, the strength of thin film metallizations are much higher and it is believed that these are applicable in industrial products. The some investigators also studied adhesion

strength after pressure cooker test, high temperature-high humidity test (85°C, 85%RH, 1000 hr.), high temperature test (150°C, 1000 hr.) and temperature cycle test (-65°C-25°C-150°C, 1000 times). The adhesion strength of NiCr/Pd/Au on AlN was hardly changed and was maintained above 2 kg/mm² after 1000 hr. or 1000 times.

Chanchani et al., at AT&T, reported the adhesion strength of Ti/Pd/Au and Ta₂N/Ti/Pd/Au systems^{15,16}. In the Ti/Pd/Au multilayer system, Ti and Pd were deposited by sputtering and gold was electroplated. Similarly, for Ta₂N/Ti/Pd/Au, Ta₂N, Ti and Pd were sputtered and then gold was formed by electroplating. Because they used 1.072 x 0.76 mm² as the pad size, their adhesion strength values can't be compared directly with those reported by Kurokawa et al.. However, high adhesion strength is obtained in both cases. Furthermore, they reported that the adhesion strength in both multilayer systems was hardly changed after aging at 85°C, 85% RH, for 1000 hr.

Drost et al. in Fraunhofer¹⁷, studied TiW/Au, NiCr/TiW/Au, and NiCr/Ni/Au multilayers and found that the combination of NiCr/Ni/Au produces the highest adhesion strength, which was 1.377 kg/mm² for a pad size of 2 x 2 mm². The layer of TiW also serves as a barrier against Au diffusion. They performed four different reliability tests of Ti/Pt/Au metallization on AlN, and measured the conductor resistance change as a function of increasing number of cycles. Their reliability test conditions are described as follows:

Temperature storage: 150°C, 1000 hr.

Temperature shock test: -65°C/150°C, 20 min./cycle, 1000 cycles

Pressure cooker test: 120°C/2 bar, 500 hr.

Humidity storage: 85°C/85%RH, 1000 hr.

They concluded that the change of the conductor resistance was below 2% for all tests.

Lodge et al. reported that NiCr/Au and Ti/Pt/Au on AlN had high adhesion strength¹⁸. Yasumoto et al., at Toshiba, studied Ti/Ni, Zr/Ni, Cr/Ni, Ta/Ni and Ni films on AlN annealed at 830°C, 5 min. in Ar atmosphere¹⁹. All metal films were deposited by sputtering methods and a 2 x 2 mm pad size was used. Except for the Ni film, a high adhesion strength of 4.5 kg/mm² was obtained.

From these studies, it was found that in all cases if Ti or NiCr is adjacent to AlN, high adhesion strength is achieved. Therefore, the adhesion mechanism between NiCr/AlN and Ti/AlN has been pursued in the recent literature.

Kurokawa et al. examined the adhesion mechanism between NiCr and AlN using Auger Electron Spectroscopy (AES)²⁰. It was found that NiCr diffusion into AlN is the main adhesion mechanism. Feil et al., in Fraunhofer, examined the adhesion mechanism using X-ray Photoelectron Spectroscopy (XPS) and High-Resolution Transmission Electron Microscopy (HRTEM)²¹. They observed a reaction zone of only 1-2 atomic monolayers between NiCr and AlN. They proposed that the presence of oxygen on the surface of AlN plays an important role for adhesion, and concluded that the adhesion mechanism was dominated by Cr-O-Al chemical bonding.

Yasumoto et al. used X-Ray Diffraction Analysis (XRD) and HRTEM to investigate the adhesion mechanism in Ti/AlN and Zr/AlN thin film

Table 5 Reaction studies between AlN and Ti.

Ti source: pure Ti thin film

Author	Suggesting reaction	Product	Annealing condition	Evaluation
Brow et al. '91 (Sandia Lab.) [23, 24]	$\text{AlN} + \text{Ti} \rightarrow \text{TiN} + \text{Al}$	TiN Al	900°C, 30 min. Ar	XPS
Yasumoto et al. [19] (Toshiba) '93	$3\text{AlN} + 4\text{Ti} \rightarrow 3\text{TiN} + \text{TiAl}_3$	TiAl ₃ (first phase) Ti ₂ N, TiN	700-950°C, 60 min. Ar	XRD

Ti source: Ag-Cu-Ti braze alloy

Loehman et al. [25, 26] (Sandia Lab.) '89	$\text{AlN} + \text{Ti} \rightarrow \text{TiN} + \text{Al}$	TiN no Al	900-1000°C, 30 min. Ar	TEM microprobe
Carim '89 [27-29] (U. of New Mexico)		TiN (Ti, Cu, Al) ₆ N	900°C, 5 min. Ar	TEM EDS
Kuzumaki et al. [31] (Tokai Univ.) '90		TiN no Al	850-950°C, 30 min. Ar	XRD microprobe
Kurihara et al. [32] (Hitachi) '92	$\text{AlN} + \text{Ti} \rightarrow \text{TiN} + \text{Al}$	TiN Al	900°C	XPS

Ti source: TiH₂(Activation agent for brazing)

Norton et al. '90 (Imperial College) [33-35]	$\text{AlN} + 5\text{TiH}_2 \rightarrow \text{Ti}_2\text{N} + \text{Ti}_3\text{Al} + 5\text{H}_2$	Ti ₂ N Ti ₃ Al	850°C, 5 min. Ar	XRD
--	---	---	---------------------	-----

General thermodynamics study

Beyers et al. [37] (Stanford Univ.) '84	$\text{AlN} + \text{Ti} \rightarrow \text{TiN} + \text{TiAl}_3$			
--	---	--	--	--

systems²². They detected the presence of aluminides, such as $TiAl_3$ or Zr_2Al , between AlN and the metal film. Because these aluminide layers have high tensile strength in the bulk materials, they concluded that aluminide layer formation was the main reason for high adhesion strength.

3.4 Reaction between AlN and Ti

Table 5 lists Ti/AlN reaction studies which have already been published. There are very few studies reported regarding the reaction between pure Ti thin films and AlN. Brow et al., in Sandia Laboratory, examined the reaction between AlN and Ti thin film using XPS^{23,24}. They deposited 80 nm of Ti on AlN with a DC sputter-deposition technique. The sample used was heated at 900°C, for 30 min., in a flowing Ar/10% H₂ atmosphere. By observation of the Ti2P and Al2P spectra, they concluded that the reaction products were TiN and Al. Yasumoto et al. formed Ti films on AlN with RF-sputtering¹⁹. The samples were annealed at 700°C, for 5 min. in Ar atmosphere. At 700°C, they found $TiAl_3$, which was the first reaction product, and then after annealing at 830°C, for 60 min., the peaks of Ti, AlN, $TiAl_3$, Ti_2N and TiN were detected with XRD. Also a gold-color was observed on the top of metal surface (TiN has a gold color).

In the case of the brazing of AlN, a Ag-Cu braze alloy containing a few percent of Ti, is usually used. It is believed that the Ti additive aids adhesion by decreasing the solid-liquid interfacial energy and improving the wettability. Because this reaction is a liquid-solid reaction and the thermodynamic activity of Ti is low, the braze alloy data can't be compared directly with the reaction between a Ti film and AlN in a quantitative sense. However, knowledge of the final reaction product between Ti in the

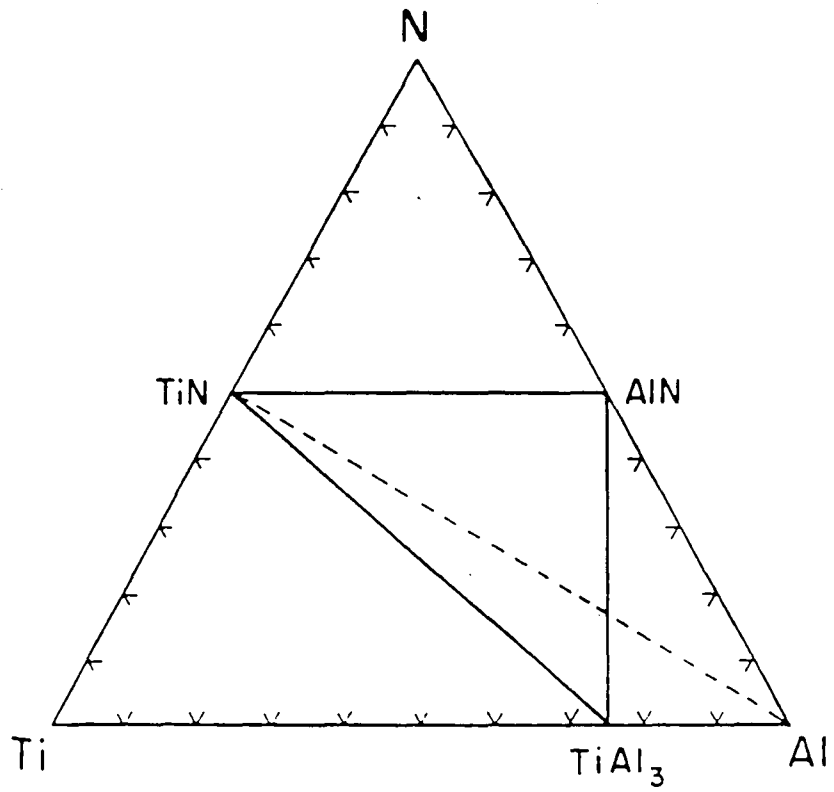


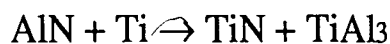
Figure 6 Phase diagram of Ti-Al-N system at 600°C. Stable(solid) and unstable(dashed) tie lines inferred from the TiN-Al and TiN-TiAl₃ reactions [37].

braze alloy and AlN is helpful for predicting the thin film reaction. Loehman et al.^{25,26}, in Sandia Laboratory, performed a reaction study of AlN and Ag-26.7Cu-4.5Ti (wt%) at 900°C for 30 min. in an Ar atmosphere. Using TEM and electron microprobe analysis, the only product they detected was TiN_{0.7}; Al was not detected at the interface between AlN and the braze alloy. Carim, at the University of New Mexico, analyzed the interface between AlN and a similar braze alloy, using TEM and X-ray Energy Dispersive Spectrometry (EDS)²⁷⁻²⁹. In a specimen annealed at 900°C for 5 min. in an Ar atmosphere, he found TiN and (Ti, Cu, Al)N₆ at the interface. This latter phase is an η family phase (M₆X) of space symmetry Fd3m. Nakahashi et al., at Toshiba, studied bonding strength and the joining mechanism to join Mo and AlN using several braze alloys, by analyzing the joints with EDS, XRD, AES, and XPS³⁰. When a Ag-Cu-Ti braze alloy was used, a high bonding strength of 19 kg/mm² was obtained by bonding at 880°C for 6min.. TiN was detected at the interface between AlN and the braze alloy using XRD. By observing the interface with SEM they concluded that the mechanism was dominated by an anchor mechanism, which is the mechanical bonding between TiN and the braze alloy. That is to say, the morphology of TiN is the key factor for high strength. They also tried to bond AlN and Mo with a Ti-Ni braze alloy, but they reported that bonding strength was extremely low. XRD showed the presence of peaks for Ni and NiTi₃, but not TiN. Kuzumaki et al., at Tokai University, used Ag-26.6Cu-5.0Ti as a braze alloy³¹. They measured the thickness of the reaction product, which was TiN, at various temperatures from 850 to 950°C, for various times from 1.5 to 30 min., using electron microprobe analysis. They reported that Al was not

observed with XRD. Kurihara et al., at Hitachi, examined the adhesion mechanism between AlN and a braze alloy containing a few percent of Ti. Using XPS and SEM³², they indicated that both TiN and Al were detected and they concluded that the high adhesion strength was achieved by an anchor mechanism for TiN, which formed between the AlN and the braze alloy. It therefore appears that in the brazing case, the major reaction product is TiN; whether Al forms or not seems to be unclear.

Norton et al., at the Imperial College, placed a TiH₂ powder layer of 10 μm thickness on an AlN surface and then set a Ag-22Cu-22Zn (wt%) braze alloy foil on top of the dispersed powder layer³³⁻³⁵. This sample was annealed at 850°C for 5 min. in an Ar atmosphere; Ti₂N and Ti₃Al were then observed with XRD.

The only detailed phase diagram available for the Ti-Al-N system was published by Schuster and Bauer in 1984³⁶ and indicates two isothermal sections, at 1000°C (1273K) and at 1300°C (1573K). These temperatures are too high in comparison to the temperatures of interest for the present study. Beyers et al., at Stanford University, reported simple schematic ternary phase diagram for Ti-Al-N at 600°C, shown in Fig. 6³⁷. According to this phase diagram, there are no tie lines between TiN and Al. Therefore, the suggested reaction is as follows:



Westwood et al.³⁸⁻⁴⁰, at Lehigh University, using TEM and AES indicate the formation of TiN, Al₂O₃ and TiAl₃ at the interface between Ti and AlN in a Au-Pt/Ti/AlN thin film metallized specimen, and indicate that the expected reaction products in an oxygen free sample should be TiN and TiAl₃ in agreement with Beyers et al..

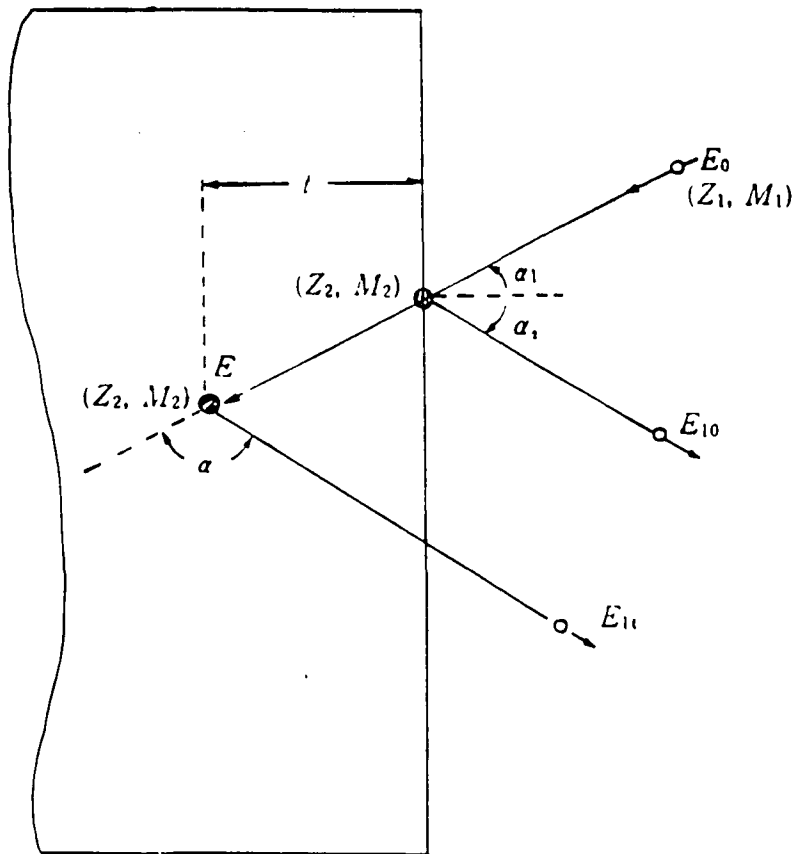


Figure 7 Schematic diagram of solid analysis by RBS [41].

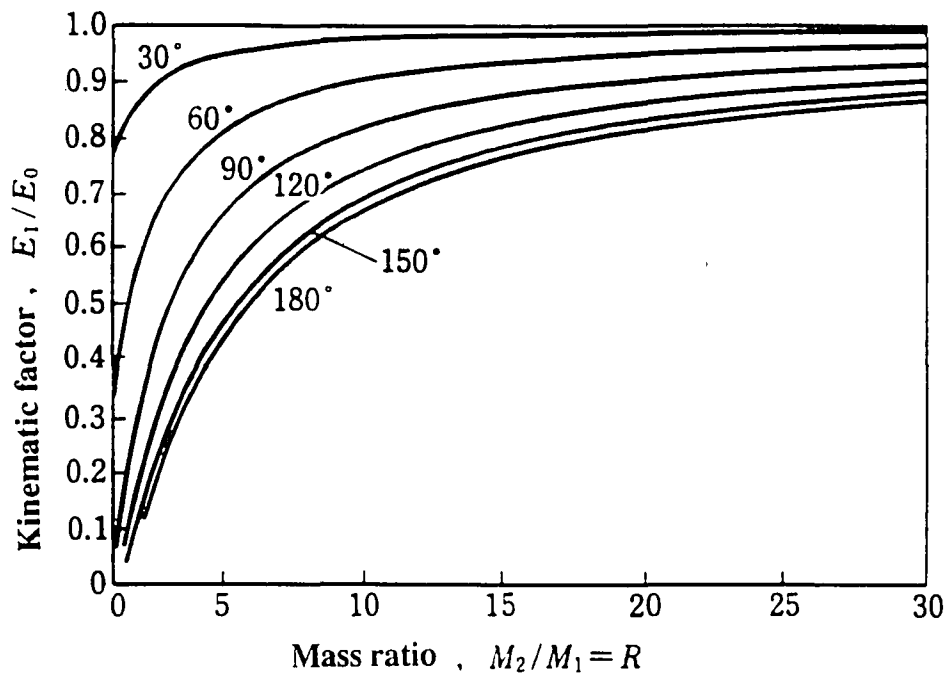


Figure 8 Relation between mass ratio and kinematic factor for various backscattering angles [41].

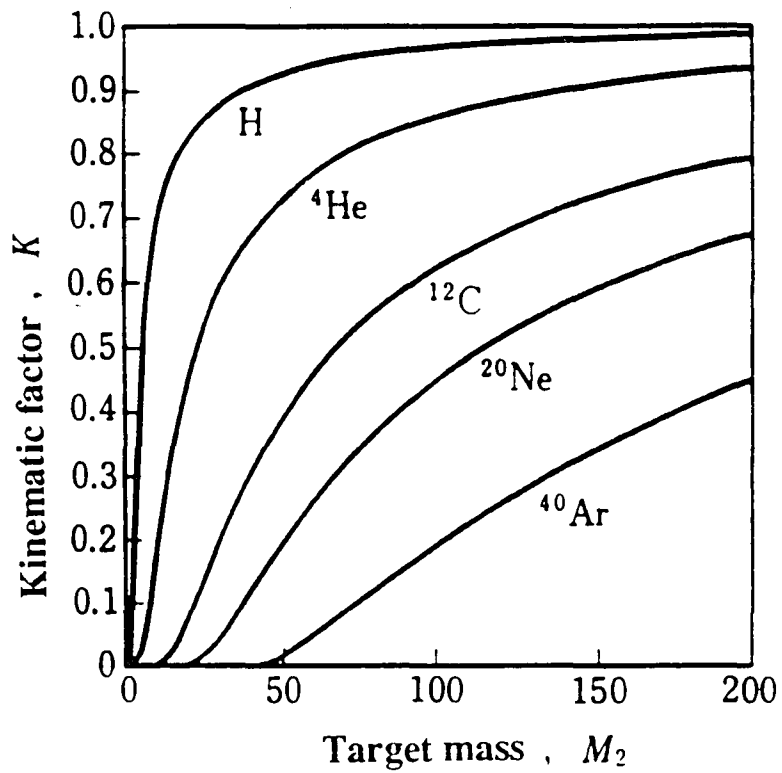


Figure 9 Relation between target mass M_2 and kinematic factor for various ion beams (Backscattering angle, $\theta=170^\circ$) [41].

3.5 Rutherford Backscattering Spectrometry (RBS)⁴¹⁻⁴⁴

RBS is a very useful technique for quantitative analysis of composition, thickness, and depth profiles of thin solid films or solid samples near the surface region. In RBS, He ions which have high energy in the order of MeVs are used as a probe. RBS is often called High Energy Ion Scattering (HEIS) because such high energy ions are used.

Supposing an ion beam is used to bombard a surface, and the ion is scattered backward by the scattering angle α , as shown in Figure 7. The back scattering ion energy can be calculated as follows:

$$E_{10} = kE_0$$

where, E_0 : incident particle energy

E_{10} : backscattering particle energy

k : kinematic factor

and the kinematic factor is given by

$$k = \left(\frac{M_1 \cos \alpha + \sqrt{M_2^2 - M_1^2 \sin^2 \alpha}}{M_1 + M_2} \right)^2 = \frac{E_{10}}{E_0}$$

Figure 8 shows the kinematic factor $k = E_{10}/E_0$ as a function of the mass ratios M_2/M_1 for various backscattering angles θ . Figure 9 shows the k factor for the specific scattering angle $\theta = 170^\circ$ when various ion beams with different atomic number are bombarded into a target having mass M_2 . These relations indicate that using an incident particle energy E_0 for an ion with mass M_1 and detector angle θ , it is possible to uniquely identify the mass M_2 at a given depth in the solid by measuring the scattered particle energy E_{10} . Figure 10 shows an RBS spectrum when He ions of energy 2.5 MeV are bombarded into a silicon substrate having a thin metal alloy layer

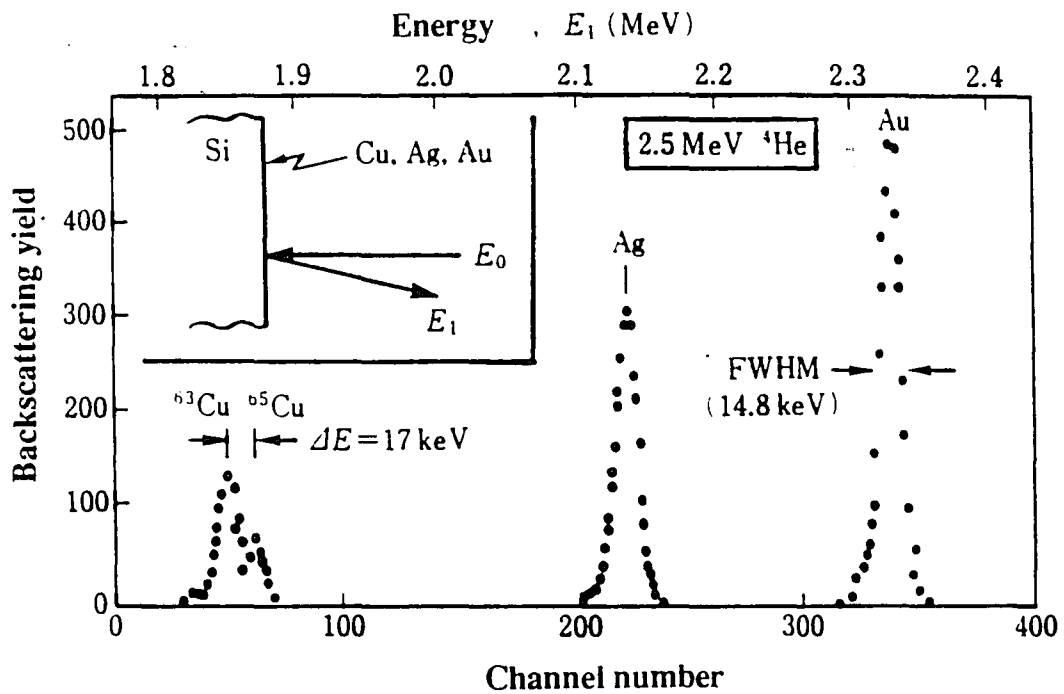


Figure 10 RBS spectrum for a thin metal layer on a silicon substrate [42].

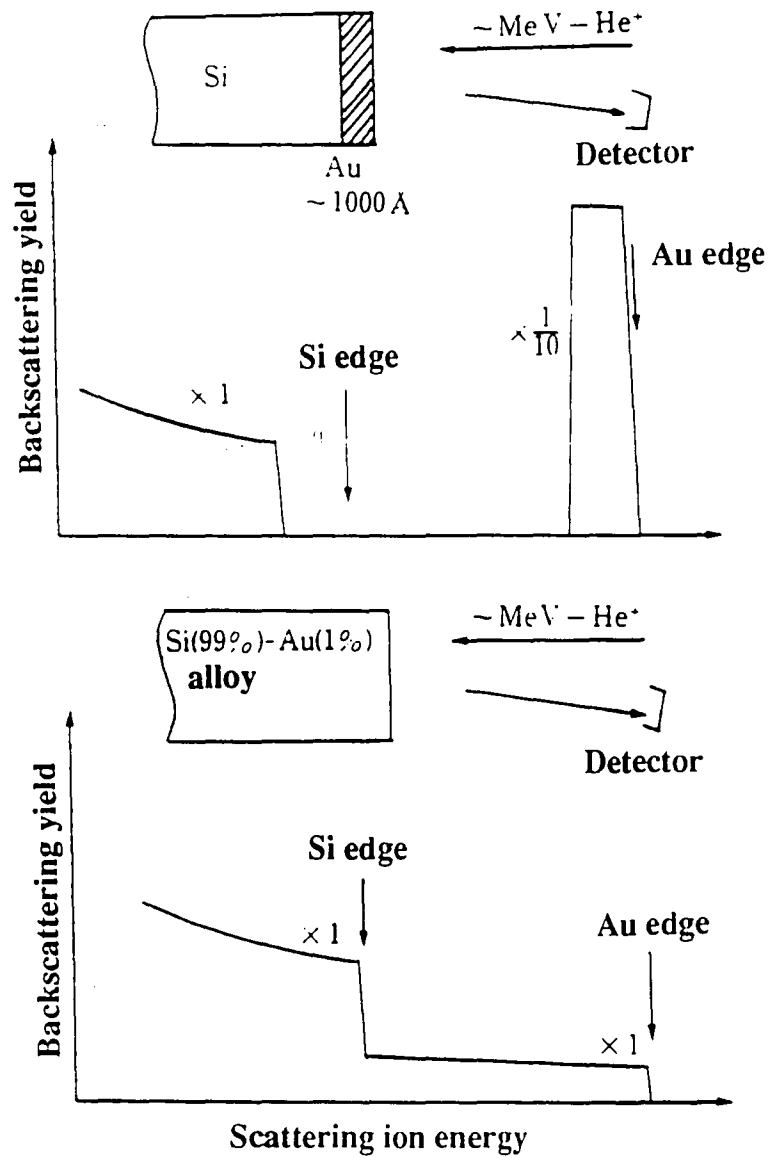


Figure 11 Example comparing the RBS spectra obtained for a gold film on a pure Si substrate (top) to that for Au distributed as a uniform impurity in a bulk alloy (bottom) [42].

at its surface, when the beam is normal to the surface. There are three peaks in the spectrum. From the energy corresponding to each peak, the kinematic factor can be calculated. Each atomic mass which is located on the surface of the silicon can be calculated, and thus Au, Ag, and Cu can be identified as the specific elements located at the Si surface.

For the case of an impurity distributed in a solid, the identification of the distributed element at a given depth can be done by including an energy loss calculation. The energy loss is the product of the stopping cross section ϵ , N and depth t . Therefore, the stopping cross section ϵ is dependent on the incident ion energy and can be expressed as follows:

$$\epsilon = -\frac{1}{N} \frac{dE}{dt} \quad (\text{eV} \cdot \text{cm}^2/\text{atoms})$$

where, t : depth

E : incident ion energy

$$N \equiv \rho \left(\frac{N_0}{M} \right)$$

ρ : density (g/cm^3)

M : mass (g/mol)

N_0 : Avogadro's number 6.023×10^{23} (atoms/mol)

The stopping cross section value ϵ is available in published tables for various combinations of ion sources and target materials. For example, we can calculate how much energy is lost when a He ion beam of 2 MeV is bombarded into Al. Because the atomic mass of Al is 26.98, N can be calculated to be 6.02×10^{22} atoms/ cm^3 . Then from the available value of ϵ ,

a value of 26.6 (eV/Å) is obtained for dE/dt . In other words, the He ions lose 26.6 eV per Å, when bombarded into Al.

Figure 11 shows a typical example helpful to demonstrate the interpretation of the RBS spectra. The figure compares the RBS spectra obtained for a gold film on a pure Si substrate (top) to that for Au distributed as a uniform impurity in a bulk Au-Si alloy. The highest energy location for the Si edge (bottom) indicates that Si is present at the surface. Comparing this to the top figure it is understood that the Si edge shown at the top represents Si just below the Au thin film. The peak in Au (top) separated from the Si edge at top indicates the Au layer to be completely separated from the Si. The overlap between the long Au spectrum (bottom) and that of Si indicates that both are present together. Roughly speaking, the spectrum is interpreted as follows: the energy level location in an RBS spectrum represents the atomic number, the width corresponds to the thickness of the film, and the height indicates the atomic ratio. Therefore, an RBS spectrum provides the compositional profile in the depth direction in easy interpretation. However, there are some drawbacks to RBS. The impurity sensitivity is greater than 10^{18} cm^{-3} , and the depth resolution of $\sim 100 \text{ Å}$ limits its use in some cases. Also, the penetration depth which can be reached is limited to around $1 \text{ }\mu\text{m}$. Moreover, the RBS spectrum doesn't provide any chemical bonding information. If the elements analyzed are close to each other in atomic number, the spectra are sometimes superimposed, making it difficult to interpret the spectrum. Despite the above given drawbacks, RBS is the most universally useful technique available for the study of interdiffusion in thin films.

4. Materials and Experimental Procedures

Tokuyama soda high purity SH-15 AlN was used as the substrate material in this study. This AlN is free of second phases typically found in AlN sintered using liquid phase sintering aids which getter oxygen. The density of this AlN substrate is 3.30 g/cm^3 . Vickers hardness is 1100 kg/mm^2 . Nominal flexural strength is $30\text{-}40 \text{ kg/mm}^2$. The thermal conductivity at R. T. is $\sim 180 \text{ W/mK}$. Thermal expansion coefficient between R. T. and 400°C is $4.4 \times 10^{-6}/^\circ\text{C}$. Volume resistivity is greater than $10^{14} \Omega\cdot\text{cm}$. The AlN was polished and lapped until it was 0.5 mm thick. The surface roughness Ra was $0.03 \mu\text{m}$.

Ti was deposited on AlN using the sputtering method. Before deposition, surface contamination was cleaned by immersion in acetone, methanol and ethanol for 3-5 min. each in an ultrasonic bath and by cleaning the surface sputtering. Normal operating procedure to assure adhesion between Ti and AlN would be to allow a temperature rise or to heat the substrate purposely during or just after film deposition. However, to minimize the reaction between the thin Ti metal film and AlN, the substrate was not heated. Depositions were made with a base pressure of $10^{-8}\text{-}10^{-9}\text{Torr}$. Three types of metal combinations were deposited by Tokuyama Soda: Ti, Ti/Ni, and Ti/Pt. One Ti/AlN sample was also deposited by DC-sputtering at Stanford University. The deposition condition used at Stanford University was as follows: Ar pressure was $3.0 \times 10^{-3} \text{ Torr}$., gun current was 200 mA (70 W) and the deposition time was 3500 sec. . The final nominal thicknesses for Ti, Ni and Pt were 1000 , 1500 and 1500 \AA , respectively, as determined by a quartz crystal monitor.

Annealing was carried out at AT&T in Reading, PA. in a pure N₂ atmosphere in a Rapid Thermal Annealing furnace (RTA), ranging from 600°C to 900°C for 15 minutes. Ramp rate was typically 75-95°C/sec.. All of the annealing conditions (including future work), are listed in Table 6.

The samples were analyzed at AT&T in Allentown, PA. by 2.25 MeV 4He^{2+} Rutherford backscattering. The detector angles of 165° and 103.5° were used in order to better obtain the mass information and the depth profile, respectively. The thickness of the compound layer was calculated from the spectra by assuming the bulk density and using the surface energy approximation in the energy loss parameter calculation. Auger Electron Spectrometry was used only to clarify the presence of whether or not oxygen is in the sample deposited at Stanford University. The depth profile through the thin film metallized layer was produced by sputtering the surface with 3 keV Ar⁺ for 15 min. at an incident angle of ~20° with respect to the surface.

Table 6 Rapid thermal annealing conditions used in this study.

Sample	Atmosphere	Temperature(°C)	Time (min.)			
Ti/AlN	as-deposited					
	Ar	725	5	10	20	40
		800	5	10	20	40
		875	5	10	15	40
		950	2	5	10	15
	N ₂	950	5			
Ni/Ti/AlN	as-deposited					
	Ar	875	5	10	20	40
Pt/Ti/AlN	N ₂	600	15			
		750				
		900				

: Samples annealed and evaluated by RBS.

: Samples in progress.

5. Results and Discussion

5.1 Reaction between Ti thin film/AlN substrate

Figure 12 shows the RBS spectrum of the as-deposited Ti/AlN specimen fabricated by Tokuyama Soda. There is no indication of any interaction between the Ti thin film and the AlN substrate. The Ti film thickness calculated by considering the bulk density (4.5 g/cm^3) is $870 \pm 50 \text{ \AA}$. A small background peak was identified as Kr present in the substrate. Although it is difficult to judge because the sputtering process condition for this sample is unclear, this interpretation is reasonable if Kr is used for the surface cleaning process of the AlN substrate before Ti deposition. Usually, in the sputter cleaning process, only inert gas is bombarded into the substrate and there is possibility that the sputtered gas is stored in the substrate. When heavy rare gases such as Kr and Xe are bombarded on ionic crystals or ceramics, it is found that these gases are trapped in the material⁴⁵. Considering this knowledge, the interpretation seems reasonable. An alternative identification for this peak is the element Yttrium, a common sintering aid for AlN. In any event, the total amount of impurity is very low. Another very few impurities are found in the spectrum, possibly Au. If the impurity is gold, the concentration is estimated at about 40 ppm atomic or 170 ppm weight.

Prior to obtaining the specimen shown in Fig. 12, we analyzed the Ti/AlN substrate deposited at Stanford University, using RBS. Figure 13 shows the RBS spectrum of the specimen. This spectrum shows the presence of a large amount of oxygen incorporated in Ti film. The oxygen concentration calculated in the Ti film is 24 ± 5 atomic percent or 10 ± 2

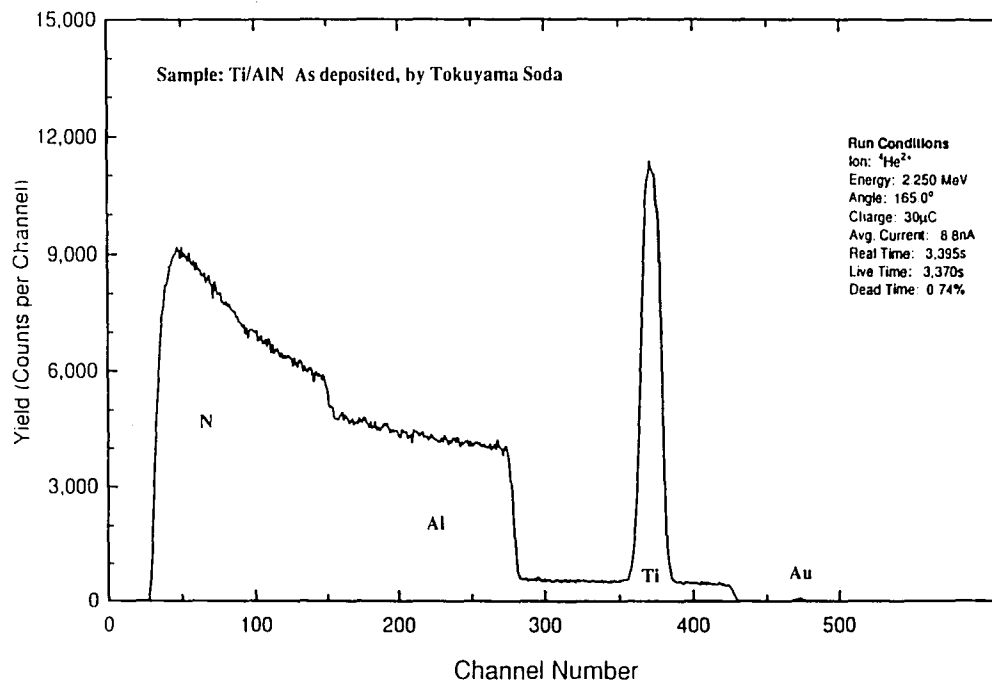


Figure 12 RBS spectrum of the as-deposited Ti/AlN specimen.

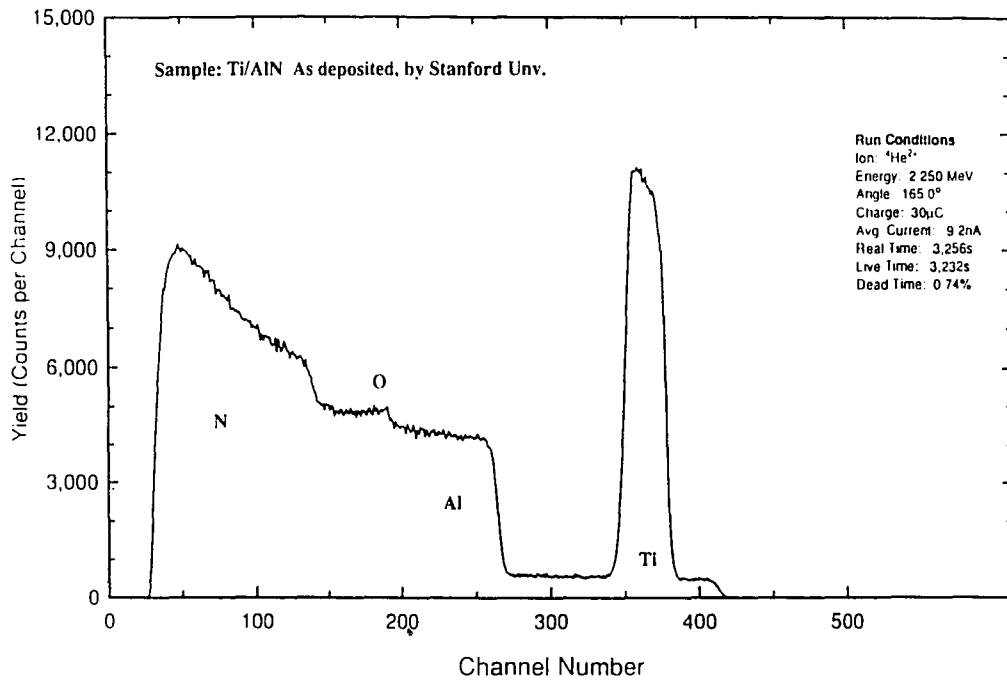


Figure 13 RBS spectrum of the as-deposited Ti/AlN specimen deposited by Stanford University.

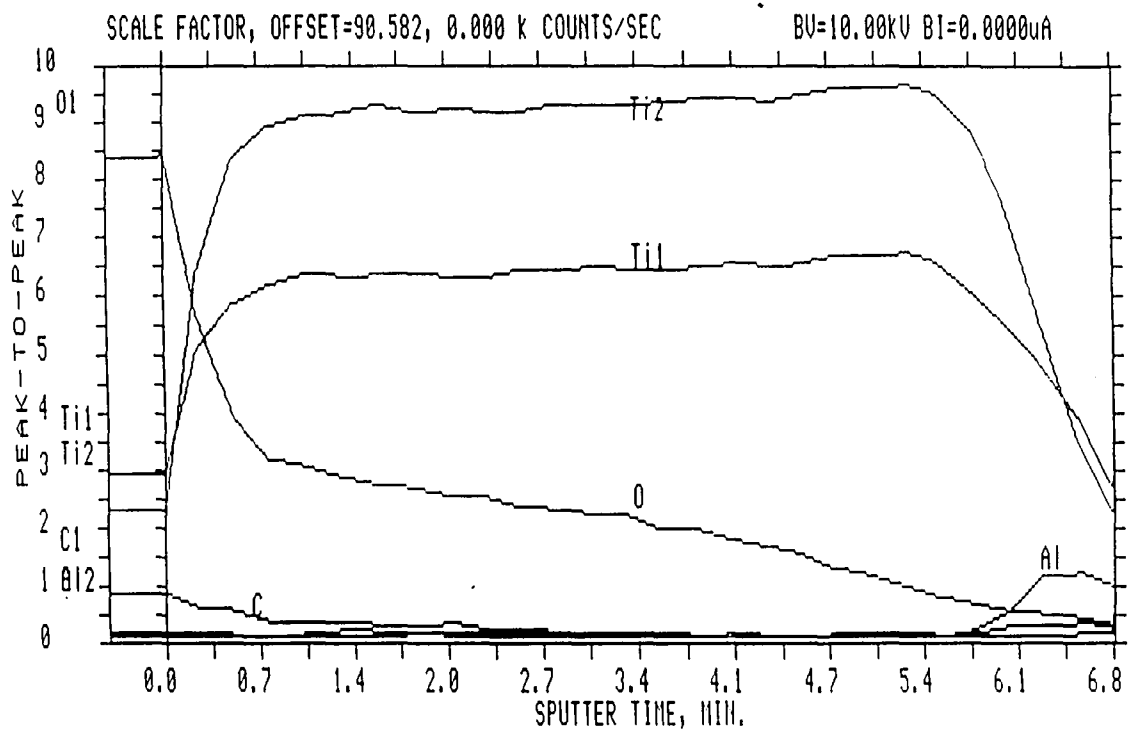
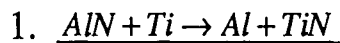


Figure 14 AES depth profile of the as-deposited Ti/AlN specimen from Stanford University.

weight percent oxygen. The Ti film thickness is $1670 \pm 150 \text{ \AA}$, based on the bulk density of Ti and ignoring any contribution due to oxygen. Another small background peak, which could be Kr or Y, also appears. To better examine the oxygen depth profile, the same specimen was analyzed using AES. Figure 14 shows the AES profiles for Ti, O, Al and C. This profile indicates that the oxygen concentration is largest on the surface and decreases slowly into the Ti film. Moreover, the oxygen does extend all the way to AlN substrate.

As future work, the samples which have non detectable oxygen as determined by RBS, will be used for the heat treatment experiment listed in Table 6, in order to obtain the interdiffusion coefficients of Ti and AlN. The annealing process should also be performed without oxygen contamination; In our first experiments, TiO₂ formation was detected due to oxygen contamination during annealing. These results are not reported here.

Although the experimental reaction diffusion study of Ti/AlN is not yet completed, we can describe the predicted reaction process in both N₂ and Ar atmosphere using thermodynamic data obtained from the literature. In the case of Ar atmosphere, it is thought that the three reactions shown below are likely to occur in the diffusion process. The Gibbs free energies of each reaction calculated using the thermodynamic data⁴⁶ are as follows:



298 – 600K

$$\Delta G_r = -25.4 - 1.61 \times 10^{-2} T \ln T + 8.35 \times 10^{-6} T^2 + 224 T^{-1} + 9.76 \times 10^{-2} T$$

600 – 932K

$$\Delta G_r = -14.9 + 1.87 \times 10^{-3} T \ln T - 2.44 \times 10^{-6} T^2 - 684 T^{-1} - 2.64 \times 10^{-2} T$$

932–1000K

$$\Delta G_T = -17.3 - 9.26 \times 10^{-3} T \ln T + 3.76 \times 10^{-6} T^2 - 684 T^{-1} + 4.65 \times 10^{-2} T$$

1000–1155K

$$\Delta G_T = -20.7 - 9.34 \times 10^{-3} T \ln T + 3.38 \times 10^{-6} T^2 - 251 T^{-1} + 5.01 \times 10^{-2} T$$

1155K –

$$\Delta G_T = -29.1 - 1.17 \times 10^{-2} T \ln T + 2.20 \times 10^{-6} T^2 - 251 T^{-1} + 7.51 \times 10^{-2} T$$

2. $AlN + 2Ti \rightarrow TiAl + TiN$

298–600K

$$\Delta G_T = -104 - 2.92 \times 10^{-2} T \ln T + 1.67 \times 10^{-5} T^2 + 601 T^{-1} + 1.91 \times 10^{-1} T$$

600–1155K

$$\Delta G_T = -93.4 - 1.13 \times 10^{-2} T \ln T + 5.94 \times 10^{-6} T^2 - 307 T^{-1} + 6.75 \times 10^{-2} T$$

1155K –

$$\Delta G_T = -110 - 1.59 \times 10^{-2} T \ln T + 3.62 \times 10^{-6} T^2 - 307 T^{-1} + 1.17 \times 10^{-1} T$$

3. $3AlN + 4Ti \rightarrow TiAl_3 + 3TiN$

298–600K

$$\Delta G_T = -226 - 6.76 \times 10^{-2} T \ln T + 4.04 \times 10^{-5} T^2 + 1120 T^{-1} + 4.39 \times 10^{-1} T$$

600–1155K

$$\Delta G_T = -195 - 1.37 \times 10^{-2} T \ln T + 8.07 \times 10^{-6} T^2 - 1600 T^{-1} + 6.72 \times 10^{-2} T$$

1155K –

$$\Delta G_T = -228 - 2.31 \times 10^{-2} T \ln T + 3.40 \times 10^{-6} T^2 - 1600 T^{-1} + 1.67 \times 10^{-1} T$$

Figure 15 shows the Gibbs free energy versus temperature curves calculated for these data. The reaction: $3AlN + 4Ti \rightarrow TiAl_3 + 3TiN$, has the

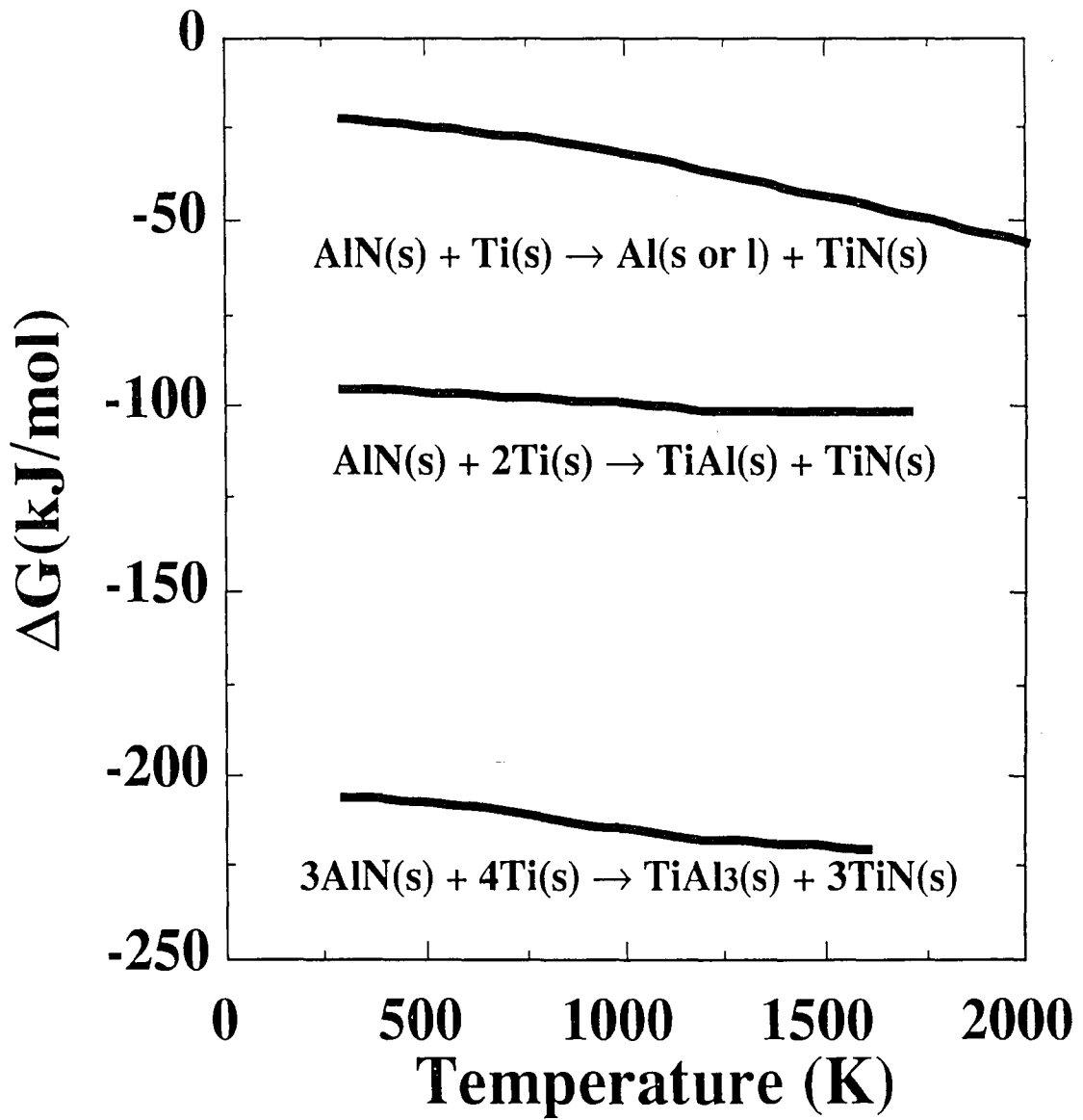


Figure 15 Gibbs free energies of the reactions concerning Ti and AlN, as a function of temperature.

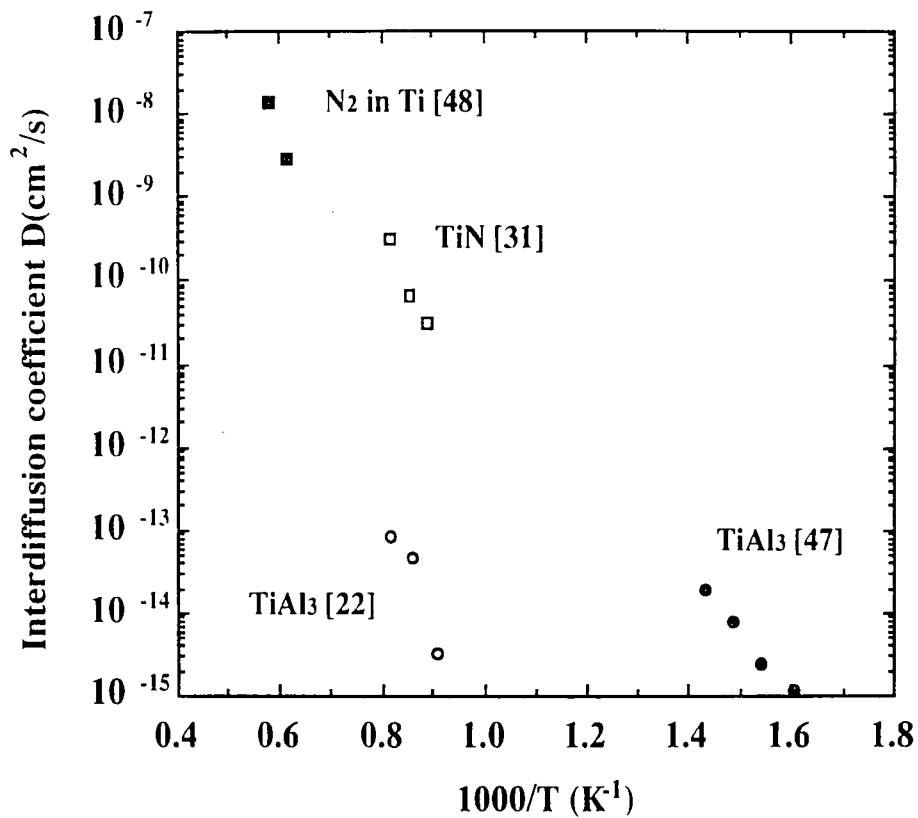


Figure 16 Interdiffusion coefficients of Ti-N, TiN and TiAl₃ obtained from literature data.

most negative value, i. e., it is the most stable reaction. The result is consistent with the conclusion reported by Beyers et al.³⁷. Therefore, in the equilibrium state, it is believed that the final reaction products are TiAl₃ and TiN.

Next, consideration of kinetic effects should be done. The interdiffusion coefficient of TiAl₃ which we consider here, is taken from Yasumoto et al.²² and Tardy et al.⁴⁷. Yasumoto et al. examined the interfacial reaction products of AlN substrates having deposited Ti thin films of 150 nm thick, after annealing ranging from 850°C to 950°C, using HRTEM and XRD. The product found was TiAl₃. They observed 50 nm of TiAl₃ at 950°C for 5 min., 38 nm at 890°C for 5 min. and 10 nm at 830°C for 5 min.. We calculated the interdiffusion coefficient of TiAl₃ using the data by assuming that diffusion produces parabolic type growth; $x^2 = \tilde{D}t$.

where, x : the thickness of the reaction product, cm

\tilde{D} : interdiffusion coefficient, cm^2 / sec

t : annealing time, sec

Tardy et al. published values for interdiffusion coefficient of TiAl₃ calculated from Ti/Al thin film couple data obtained using XRD and RBS. Both results are shown in Fig. 16. There is a large difference between both sets of results. Interdiffusion coefficient data for TiN is taken from the studies of Kuzumaki et al.³¹ and that of nitrogen in α -Ti is taken from Bars et al.⁴⁸. Kuzumaki et al. studied the thickness of the interfacial product formed between AlN and a Ag-Cu-Ti braze alloy. Because the only product TiN was found, the thickness dependence on annealing time and temperature were again used to calculate the interdiffusion coefficient of TiN. However, the values calculated must be taken with some skepticism,

because the Ti activity is small this case. In the paper reported by Bars et al., the interdiffusion coefficient of nitrogen in α -Ti was deduced by studying the diffusion between Ti and nitrogen. The interdiffusion coefficients for TiN and for Ti-N are also plotted in Fig. 16. Both data sets are consistent and can be extrapolated by the same line.

From this figure, it is understood that the interdiffusion coefficient of TiN is approximately three folds less than that of TiAl₃ in Yasumoto et al.. That is to say, the formation of TiN is much faster than that of TiAl₃. If growth is estimated from the reaction between Ti and AlN using the thermodynamic and kinetic data described above, the prediction is as follows: initially, TiN is formed at the interface and then TiAl₃ is formed. This prediction doesn't agree with the result of Yasumoto et al., because they reported that the first compound formed was TiAl₃. However, the extrapolation line of the interdiffusion coefficients for TiAl₃ reported by Tardy et al. when projected to higher temperature fits closely to both the Ti-N and TiN interdiffusion coefficient data. Therefore, if the study of Tardy et al. is adopted, it is difficult to determine which product is the first expected to form.

Also in the case of nitrogen atmosphere, if we adopt the data from Yasumoto et al. rather than Tardy et al., TiN is first formed on top of the Ti surface, by reaction with nitrogen, and then TiN is formed at the interface between Ti and AlN by reaction of Ti and AlN; after that, TiAl₃ is formed at the interface. However, these predictions are for the case using a semi-infinite Ti/AlN couple and consider the equilibrium state. In the case of a thin Ti film, it is possible that TiAl₃ may not appear, because TiN growth continues until some critical thickness and this critical thickness could be

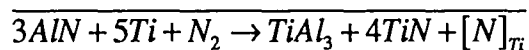
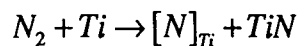
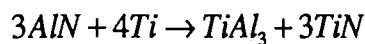
greater than the thin film thickness itself. Similar to the situation considered for the Ar atmosphere case, if growth obeyed the data from Tardy et al., it is hard to judge the first reaction product and reaction sequence.

For the sake of argument, it is also possible to consider an alternative and less sure interpretation. Figure 17 shows additional interdiffusion coefficient data for Ti-N, TiN and Al-Ti taken from other literature data⁴⁹⁻⁵¹. For (α -Ti)-N, many diffusion studies have been reported. Figure 18 shows these (α -Ti)-N interdiffusion coefficient data as summarized by Anttila et al.⁴⁹ together with his experimental results. There is some data spread, specially at temperatures greater than 850°C, in terms of the line slope (as activation energy). However, as far as the values are concerned, these data are consistent and can be extrapolated by the same line. By adding the (α -Ti)-N diffusion data of Anttila et al., which covers the low temperature range, it is noted that the slope of the line is constant and is steeper than the extrapolation through the low temperature TiAl₃ data of Tardy et al.⁴⁷ as shown in Fig. 17.

On the other hand, the interdiffusion coefficients for Ti-Al are very scattered (Fig. 17). It is therefore very difficult to judge between these Ti-Al diffusion data. Therefore, we could make one of two alternative assumptions. One is that these Ti-Al data are divided into two groups: the data taken by Pokoev et al.⁵⁰ and Tardy et al.⁴⁷, and that by Yasumoto et al.²² and Raisanen et al.⁵¹. However, it is unknown why two sets of diffusion data would exist. Several alternative assumptions could be that there is larger spread and deviation due to several unidentified experimental errors. If the second alternative is adopted and the line for all

these Ti-Al data are drawn by calculation using the least square method, the line is shallower shown in Fig. 17 is obtained. From Fig. 17, it is noted that there is a cross-over in the two lines $1000/T \sim 1.2$ ($T \sim 830^\circ\text{C}$). That is to say, below 830°C , Ti-Al diffusion is faster than Ti-N, and above 830°C Ti-N is faster than Ti-Al. At low temperature, TiAl_3 is likely to form. Although this interpretation is relatively bold, several literature papers support this idea. Rao et al.⁵² reported that the reaction between an Al film 0.5 to 1.0 micron thick and a thick Ti substrate forms TiAl_3 very rapidly on heating to 635°C , but after heating to 900°C , Ti_3Al is formed. Also if we examined Table 5, it is found that only Yasumoto et al., who performed experiments at low temperature (700°C), observed TiAl_3 . As a result, this above interpretation appears to be reasonable. If this interpretation is correct, the first product to form between Ti/AlN is dependent on temperature. At low temperature below around 830°C , TiAl_3 is formed first. At higher temperature, TiN is formed first. This approach provides a more flexible view in terms of the interpretation of the AlN-Ti reaction.

Furthermore, if we take into account the solubility of nitrogen in Ti, the reaction can be described as follows:



Because the Gibbs free energy of the reaction $1/2\text{N}_2 \rightarrow [\text{N}]_{\text{Ti}}$ is $\Delta G = -283570 + 100.6T$ (J/mol)⁵³, the Gibbs free energy of the reaction $3\text{AlN} + 5\text{Ti} + \text{N}_2 \rightarrow \text{TiAl}_3 + 4\text{TiN} + [\text{N}]_{\text{Ti}}$ at 1000K is -640.7 kJ/mol. The value is less than that of $3\text{AlN} + 4\text{Ti} \rightarrow \text{TiAl}_3 + 3\text{TiN}$ (see the value at 1000K in Fig.

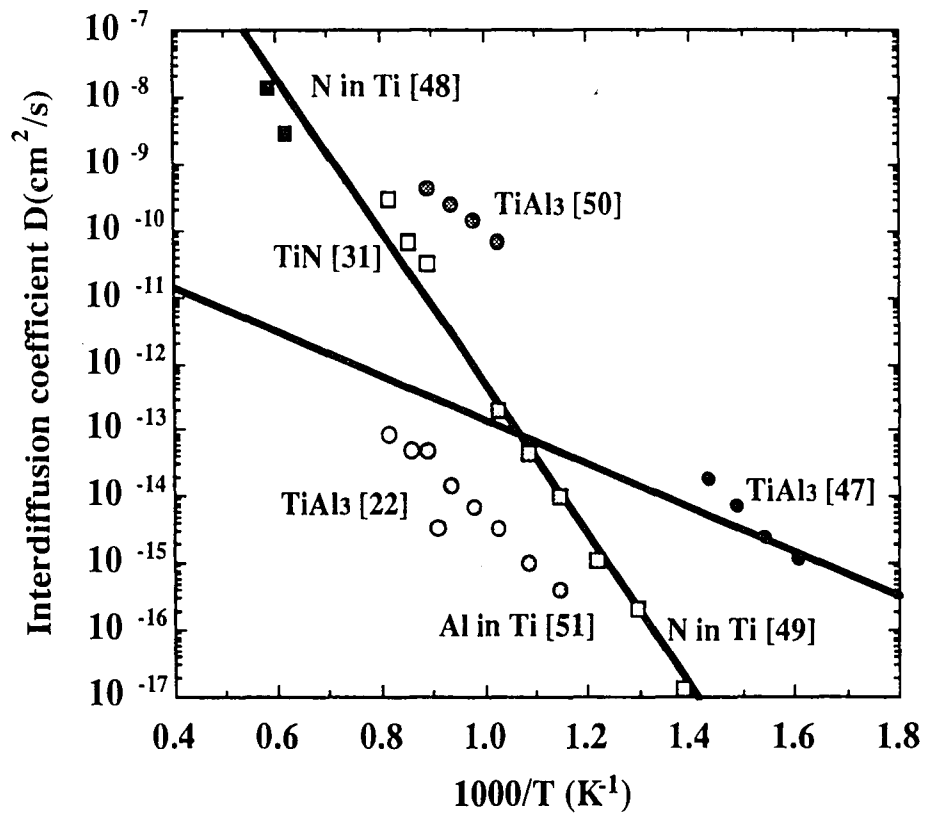


Figure 17 Interdiffusion coefficients of the Ti-N and Al-Ti reactions from the literature.

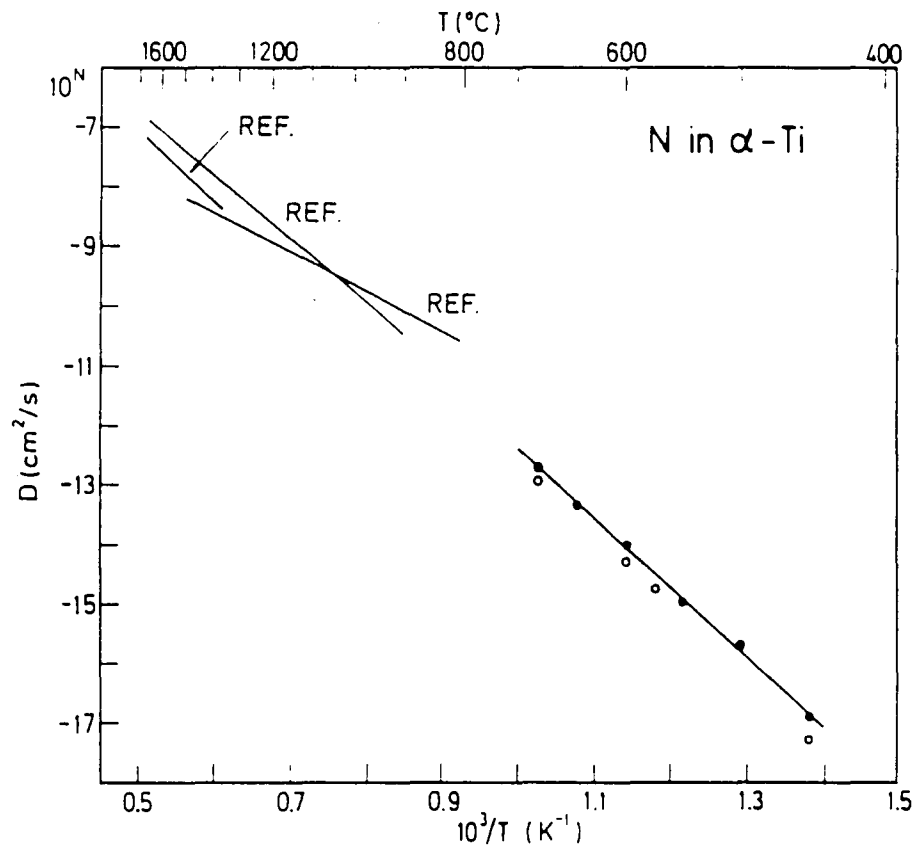


Figure 18 Comparison of the Arrhenius plots for nitrogen diffusion in α -Ti [49].

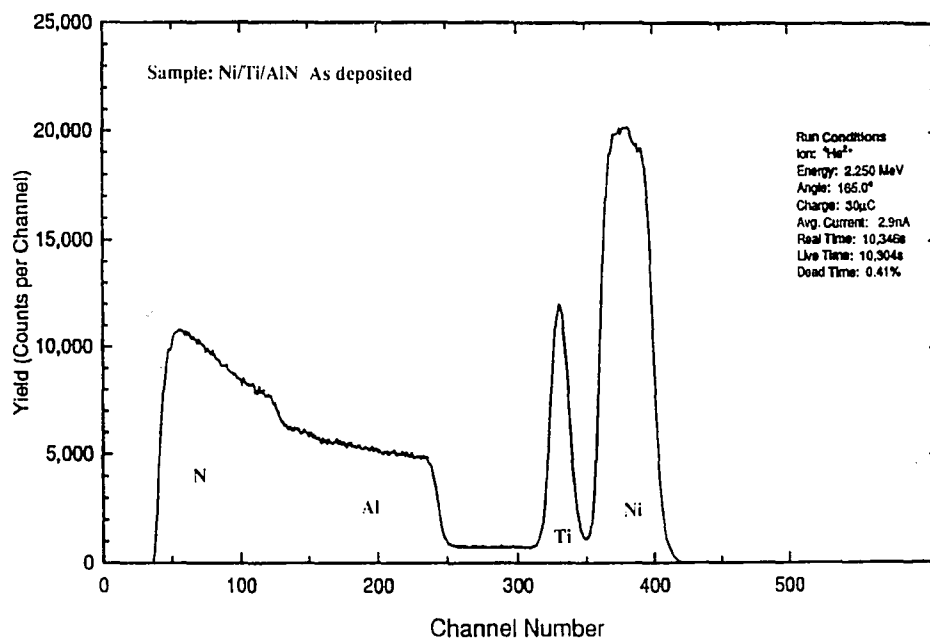


Figure 19 RBS spectrum of the as-deposited Ni/Ti/AlN specimen.

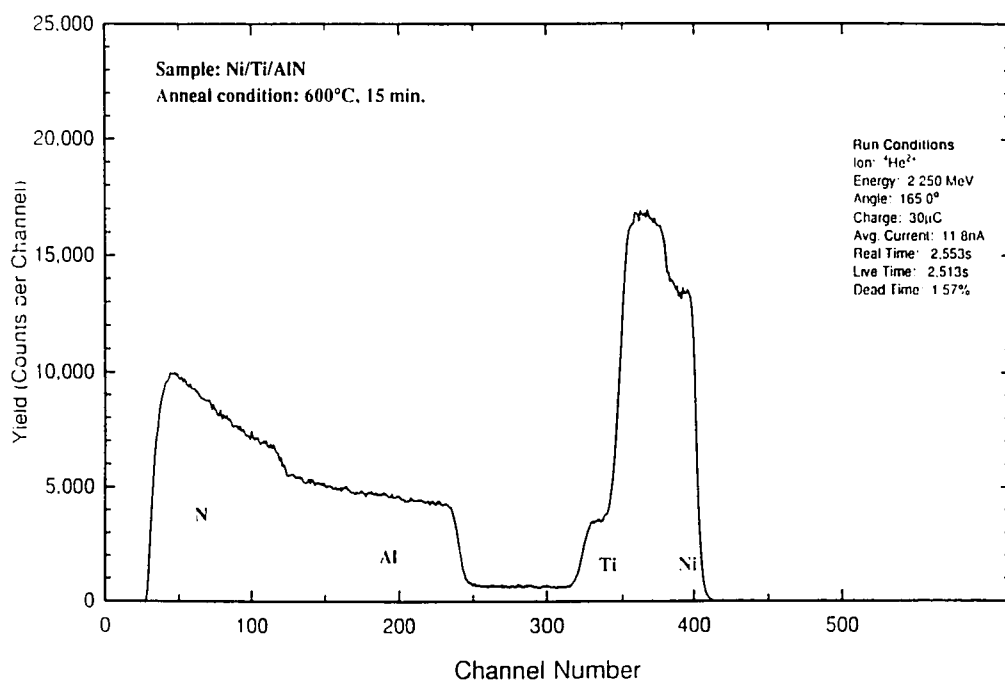


Figure 20 RBS spectrum for the Ni/Ti/AlN specimen annealed at 600°C for 15 min. in N₂ atmosphere.

15). It appears that the reaction considering the solubility of nitrogen is more stable.

5.2 Reaction between Ni/Ti/AlN substrate

Figure 19 shows the RBS spectrum of the as-deposited Ni/Ti/AlN sample. The Ni and Ti peaks are well separated, and it is found that there are no reactions between Ni, Ti, and AlN. The sample has $920 \pm 80 \text{ \AA}$ of Ti under $1510 \pm 120 \text{ \AA}$ of Ni. From the background between the Ti and AlN peaks, there is 0.85 ± 0.04 atomic percent (3.4 ± 0.1 weight percent) Kr(?) in the AlN, similar to that observed in the spectrum for Ti/AlN. Figure 20 is the RBS spectrum of Ni/Ti/AlN annealed at 600°C for 15 min. in nitrogen atmosphere. The figure shows that after annealing at 600°C , the Ti and Ni layers have completely interdiffused. The Ti/Ni ratio is 0.30 ± 0.01 . The Ni concentration is 76.8 ± 0.4 atomic percent or 80.2 ± 0.4 weight percent. The Ti concentration is 23.2 ± 1.0 atomic percent or 19.8 ± 0.8 weight percent. The effective $\text{NiTi}_{0.3}$ layer number is $1.41 \times 10^{18} \text{ NiTi}_{0.3}/\text{cm}^2$, although the exact thickness cannot be calculated because the density of $\text{NiTi}_{0.3}$ is unknown. There is no change in the AlN substrate.

Figure 21 shows the RBS spectrum of the specimen annealed at 750°C for 15 min. in a nitrogen atmosphere. After the 750°C anneal, the Ti continues to diffuse through the Ni layer and starts to react with nitrogen in the atmosphere to form a surface TiN layer. Based on the normal TiN bulk density, which is 5.43 g/cm^3 , the film is $320 \pm 30 \text{ \AA}$ thick. The Ti concentration in the Ni has dropped to 16.3 ± 1.0 atomic percent, or 13.7 ± 0.8 weight percent. The Ti/Ni ratio of the specimen is 0.20 ± 0.01 . The Ni concentration is 83.7 ± 0.4 atomic percent, or 86.3 ± 0.4 weight percent.

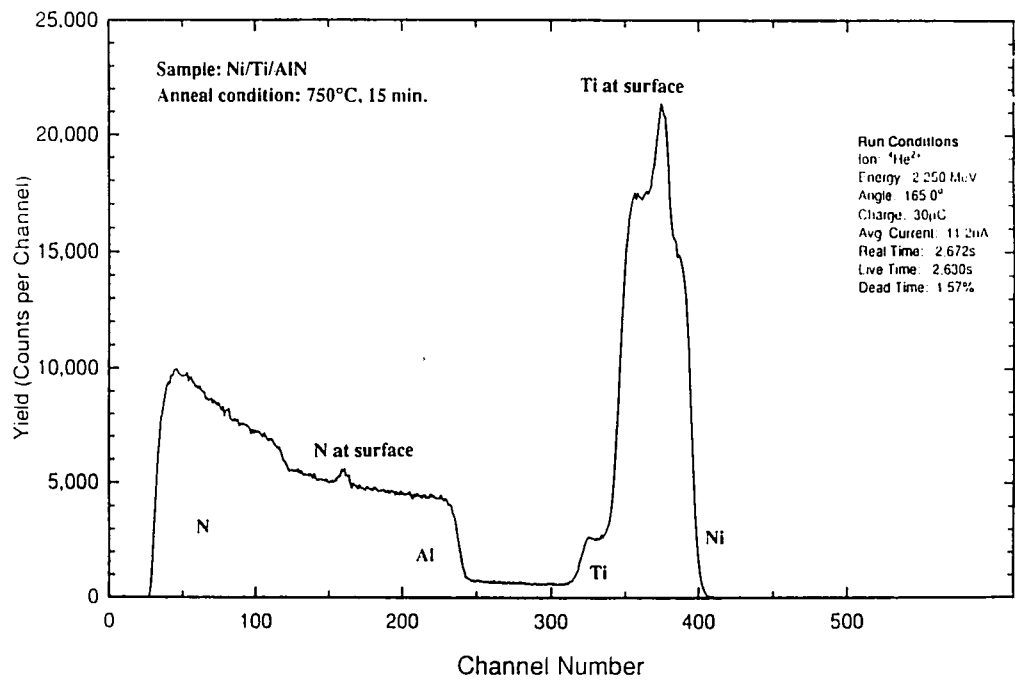


Figure 21 RBS spectrum of the Ni/Ti/AlN specimen annealed at 750°C for 15 min. in N₂ atmosphere.

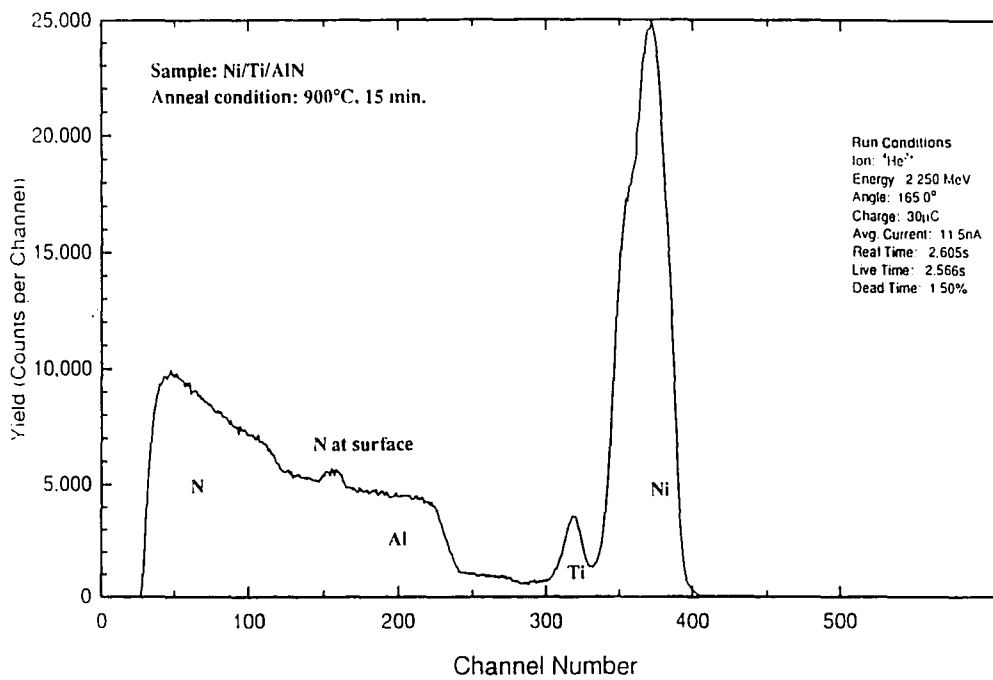


Figure 22 RBS spectrum of the Ni/Ti/AlN specimen annealed at 900°C for 15 min. in N₂ atmosphere.

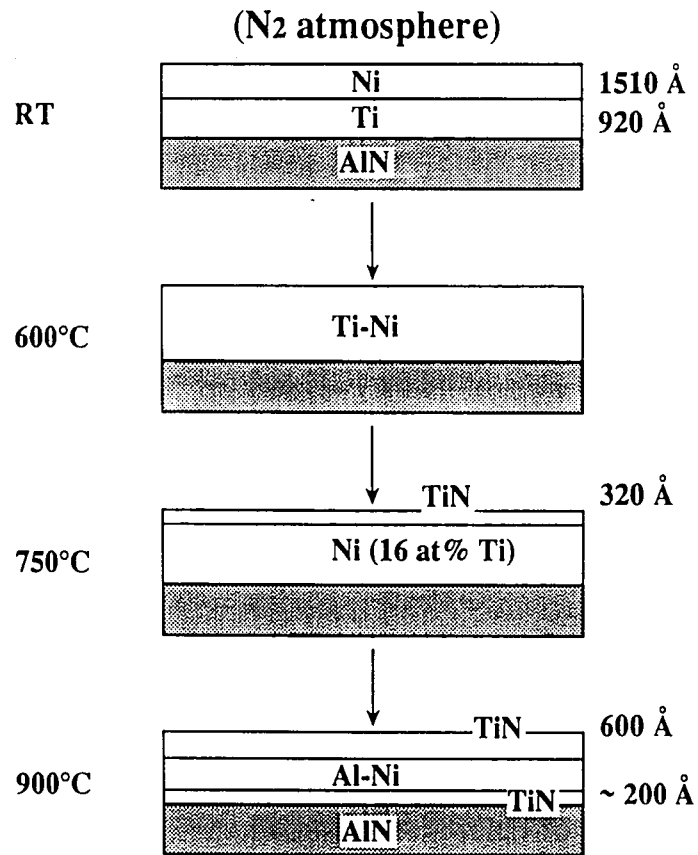


Figure 23 Schematic diagram of Ni/Ti/AlN diffusion and reaction sequence in N₂ atmosphere as a function of temperature.

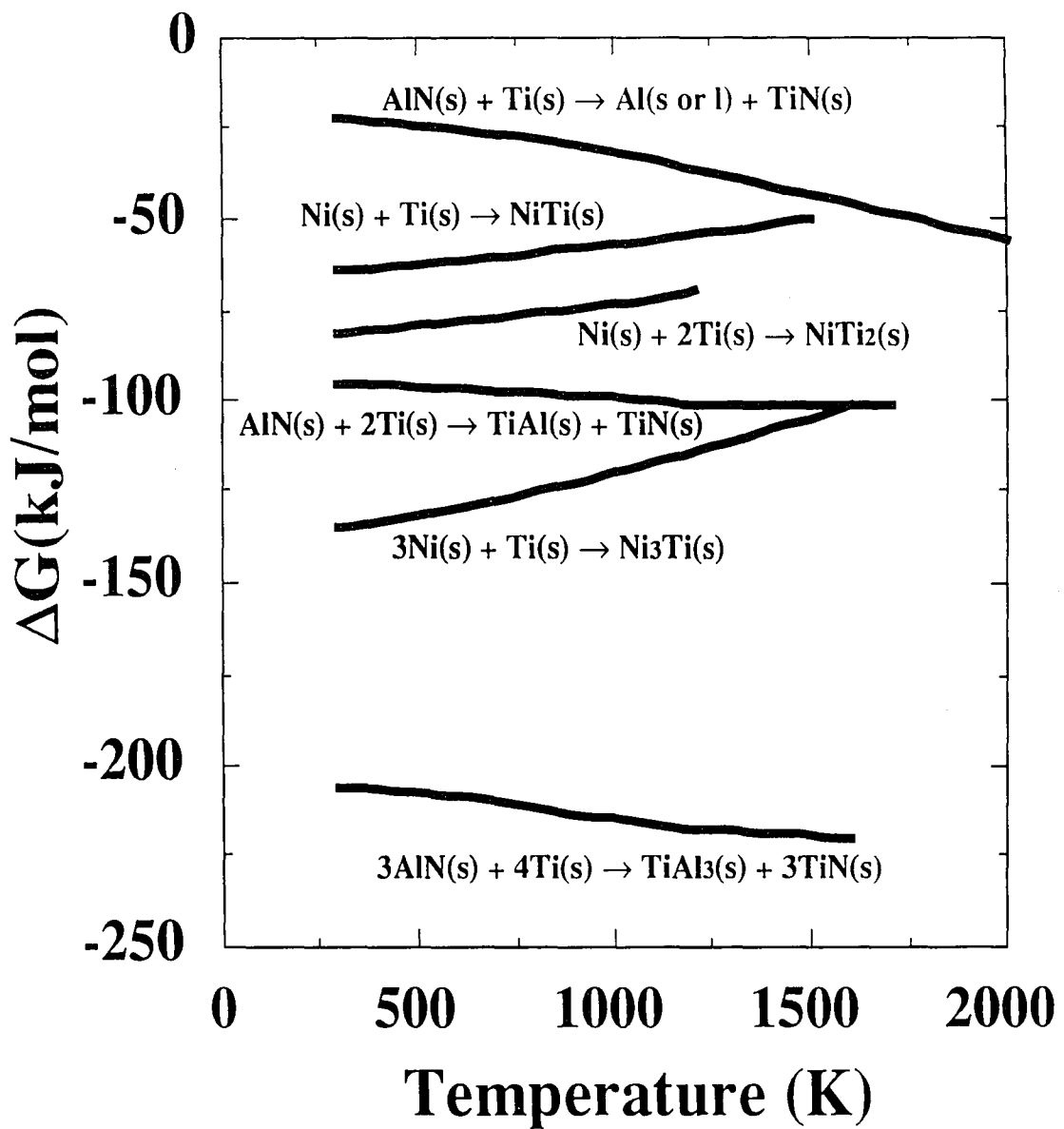


Figure 24 Gibbs free energies for reactions involving Ni/Ti/AlN, as a function of temperature.

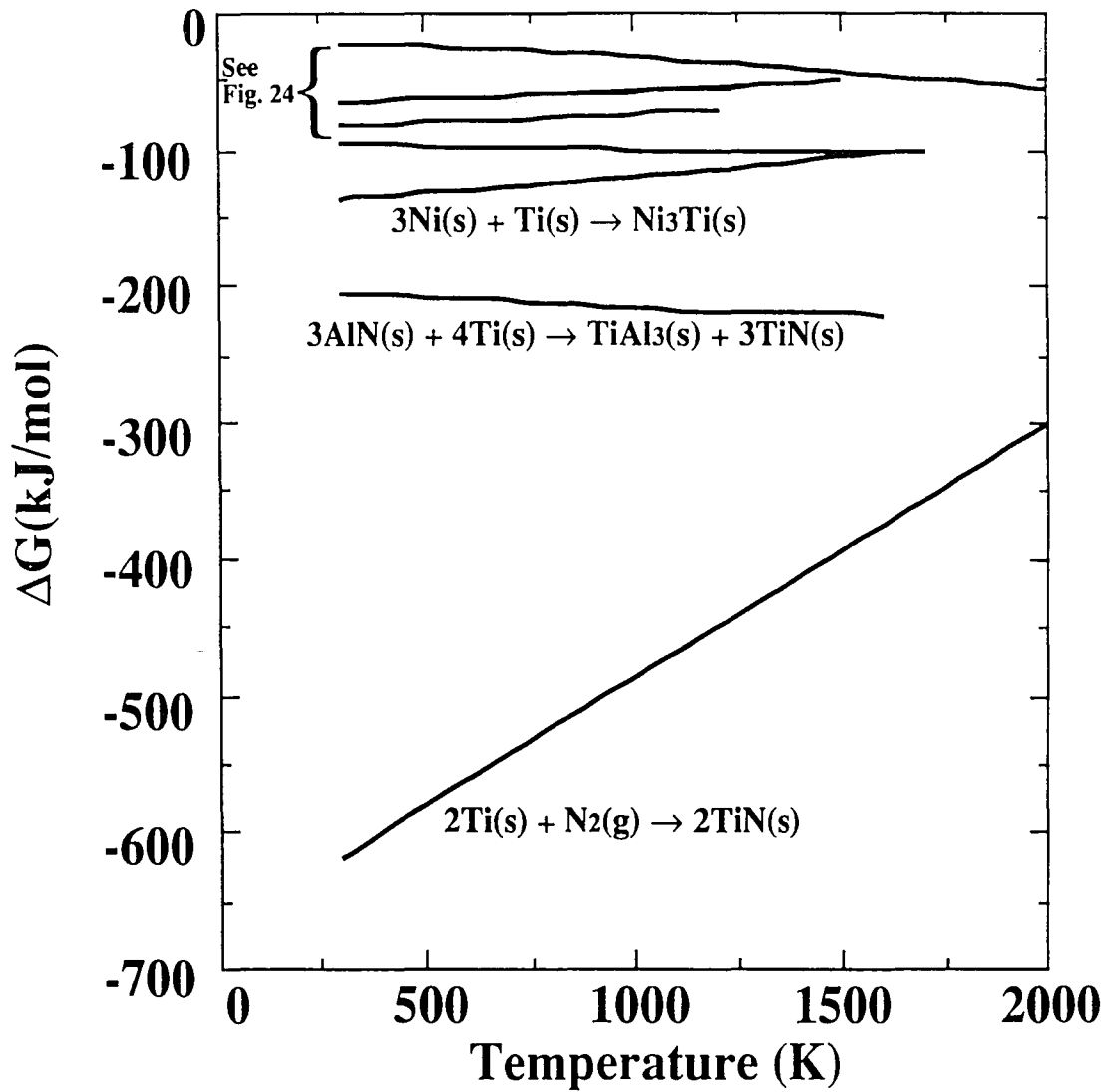
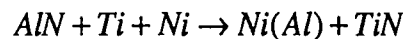


Figure 25 Gibbs free energies for reactions involving Ni/Ti/AlN, and considering the reaction with atmosphere.

The effective NiTi_{0.2} layer number is 1.40×10^{18} NiTi_{0.2}/cm². The amount of Ti required to produce the TiN film is in good agreement with the decrease in the Ti concentration in the NiTi_{0.2} film.

Figure 22 shows the RBS spectrum of the specimen annealed at 900°C for 15 min. in a nitrogen atmosphere. After annealing at 900°C, the surface TiN layer has grown to a thickness of 600 Å. Al has now diffused into the Ni. The Al concentration in the Ni-Al layer is 5.9 ± 0.6 atomic percent or 2.8 ± 0.3 weight percent, while the Ni concentration is 94.1 ± 0.5 atomic percent or 97.2 ± 0.5 weight percent. There is no longer any measurable Ti in this layer. A thin layer of TiN (210 Å) is now present adjacent to the AlN. The presence of Al in the Ni layer and the formation of the TiN layer adjacent to AlN indicates that the reaction between Ti and AlN has now started, the products being TiN, and Al which has diffused into the Ni layer. The complete reaction may be:



A schematic diagram of the reaction sequence summarizing these above RBS results is shown in Fig. 23. An important thing to note is the Ti diffusion behavior: at 600°C, Ti reacts with Ni instead of reacting with AlN; at 750°C, TiN is formed on the top of surface. Because nitrogen atmosphere was used in this study, it seems that Ti reacts rapidly with the nitrogen atmosphere. From the above description, it is understood that the interdiffusion reaction of Ni/Ti is faster than the reaction-diffusion of Ti/AlN. Also, it is estimated that the reaction of Ti/N lies between Ni/Ti and Ti/AlN in terms of reaction kinetics.

These results may be considered with respect to both thermodynamics and kinetics. Figure 24 shows the Gibbs free energy curves as a function of

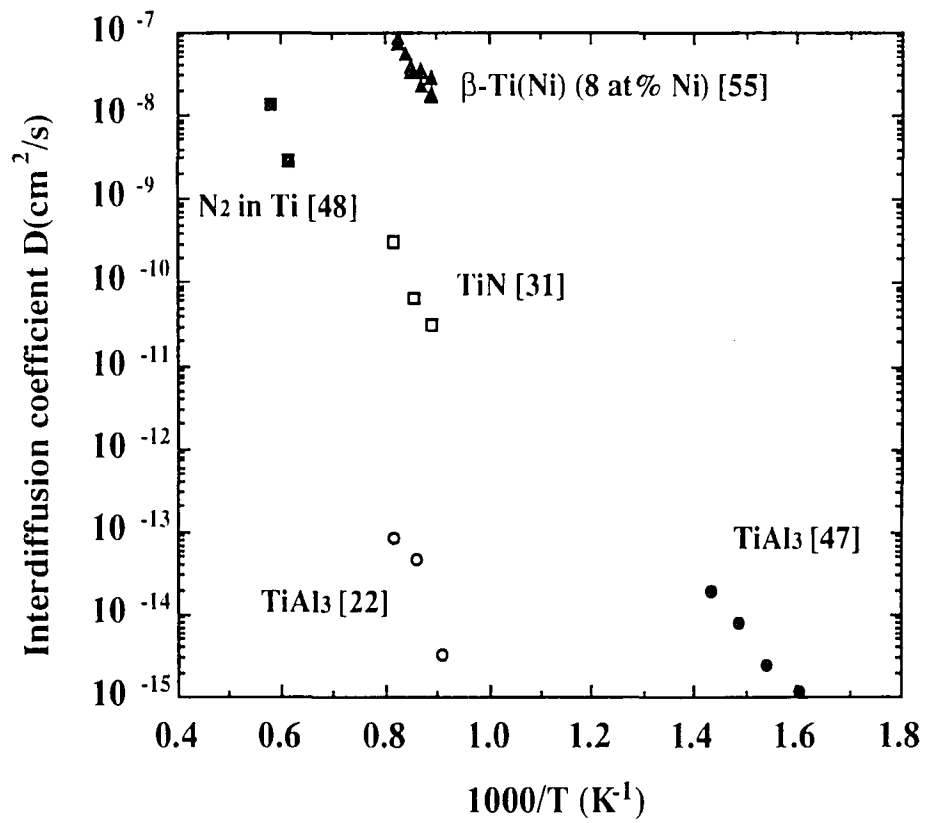


Figure 26 Arrhenius plot of the interdiffusion coefficient regarding Ni/Ti/AlN reactions.

temperature with regard to the expected reactions between Ni/Ti and AlN. The reaction of Ti and N is added in Fig. 25. If we also consider the effect of the N₂ atmosphere, the reaction $2Ti + N_2 \rightarrow 2TiN$ has the most negative value, which means this product is the most stable in this system. However, reactions of AlN/Ti, and Ni/Ti also have negative values. Our diffusion results are not for a system at an equilibrium state, but are for a system going to the equilibrium state. Therefore, it cannot be determined which reaction takes place first from thermodynamics, although it is found that all of the above three type of reactions can occur, because all three reactions possess a negative Gibbs free energy value. An Arrhenius plot of pertinent interdiffusion coefficients is shown in Fig. 26, and is revised from Fig. 16 by adding the interdiffusion coefficient literature data regarding the Ni-Ti reaction. The Ni-Ti diffusion data is taken from the results reported by Bastin^{54,55}. For simplicity, if the TiAl₃ interdiffusion coefficient reported in ref. 22, is adopted, it is found the relative magnitude of the diffusion rates can be described in the following way:

$$D_{Ni-Ti} > D_{Ti-N} > D_{AlN-Ti}$$

These literature diffusion literature data indicate good agreement with our experimental results. In addition, the work reported by Nakahashi et al.³⁰ support our proposed reaction scheme. They studied joints of AlN/Mo using several braze alloys in various annealing conditions. When Ti foil of 3 μm thickness was inserted between Cu foil of 100 μm thickness and AlN (i. e., the braze alloy is Cu-Ti), TiN was observed at the AlN/braze alloy interface after 1050°C, for 6 min. (Formation of TiN caused a high bond strength.). However, when Ni foil of 100 μm thickness was used instead of Cu foil, TiN was not observed at the interface, after 1100°C for 6 min., but

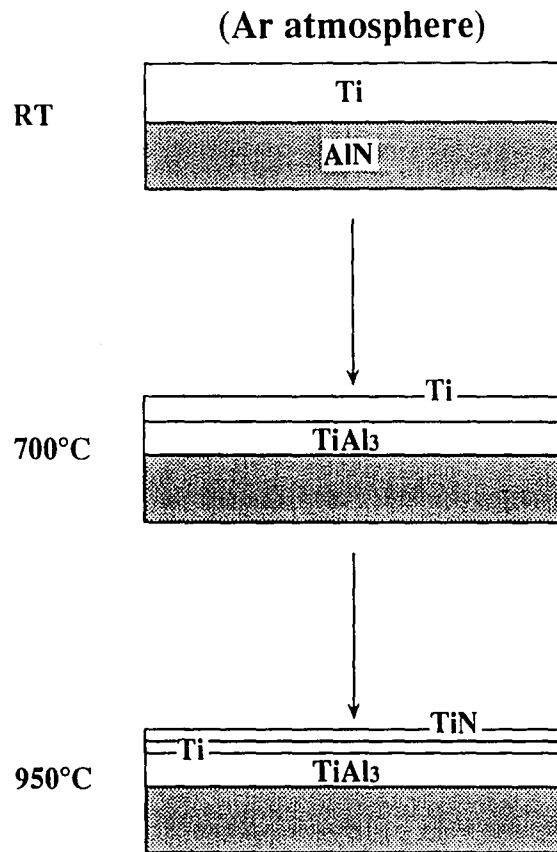


Figure 27 Schematic diagram of the reaction of Ti/AlN annealed in Ar atmosphere [19].

instead Ni₃Ti was detected by XRD. In the joint interface region between AlN and the braze alloy, wetting was extremely poor and the bond strength was almost zero. That is to say, they also observed that Ti reacted with Ni instead of AlN when Ni and AlN are adjacent to Ti.

Here, for its industrial interest, we again introduce the study of Yasumoto et al.¹⁹ more. Figure 27 shows the reaction sequence summary between Ti and AlN in an Ar atmosphere, as reported by Yasumoto et al.. They propose that the formation of TiAl₃ at the interface causes high adhesion strength. According to their study, TiAl₃ is obtained by reaction between Ti and AlN. Our results show that Ti doesn't react strongly with AlN in the case of Ni/Ti/AlN. Therefore, in order to obtain a TiAl₃ layer at the Ti/AlN interface in a Ni/Ti/AlN combination, the heat treatment should be performed during Ti deposition or just after Ti deposition, and then the Ni film must be deposited on the Ti film. In other words, it appears that formation of a TiAl₃ layer requires a two step thin film process. As shown in Fig. 27, TiN is formed on the top surface even in the case of an Ar atmosphere heat treatment. In this case nitrogen in the TiN comes from AlN. To better understand this atmosphere effect, further study as listed in Table 6 will be necessary.

5.3 Reaction between Pt/Ti/AlN substrate

Figure 28 shows the RBS spectrum for the as-deposited Pt/Ti/AlN sample. The Pt and Ti peaks are well separated and no interdiffusion between Pt/Ti/AlN can be observed from the spectrum. It is found that the sample has 1230 ± 100 Å of Ti under 1130 ± 100 Å of Pt. Also, in this sample, the background several energies just above the AlN peak indicate

the presence of Kr(?). In the specimen annealed 600°C for 15 min. shown in Fig. 29, Ti has started to diffuse through the Pt and the concentration of Ti at the outer-surface is 8 ± 0.5 atomic percent or 2.1 ± 0.1 weight percent. No Al movement was observed. Figure 30 shows the superimposed RBS spectra of the specimens annealed at both 750°C and 900°C. For the specimen annealed at 750°C, both Al and Ti diffused into Pt. At the outer-surface, the concentration of Ti is estimated to be 30.9 ± 0.5 atomic percent or 10.5 ± 0.2 weight percent. The concentration of Al at the outer-surface is 5.3 ± 0.8 atomic percent or 1.0 ± 0.2 weight percent. At the Pt-Ti interface, the Ti concentration is 33.7 ± 0.5 atomic percent or 11.8 ± 0.2 weight percent. The Al concentration at the Pt-Ti interface is the same as the value at the surface. The rise in peak height at the lower end of the Ti peak region indicates a local increase in Ti at the original Ti/AlN interface. For 900°C anneal, both Al and Ti have diffused into the Pt film. The Ti concentration at the center of the Pt film is estimated to be 26.3 ± 0.5 atomic percent or 8.4 ± 0.1 weight percent, and the Al concentration is 3.5 ± 0.8 atomic percent or 0.6 ± 0.1 weight percent. Unlike at 750°C, TiN is formed at the specimen surface at 900°C. It is believed that the nitrogen is provided from the ambient atmosphere. The TiN thickness is about 250 Å.

Figure 31 shows the schematic diagram of the reaction sequence summarizing the results for Pt/Ti/AlN. It is noted that Ti diffuses into Pt, not into AlN, similar to the Ni/Ti/AlN diffusion case. In other words, the interdiffusion rate between Pt/Ti is faster than that between Ti/AlN. Also similar to the Ni/Ti/AlN case, TiN is formed on the top surface. Study of

the comparison between reactions in nitrogen and in argon atmosphere should be performed in Pt/Ti/AlN specimens, as outlined in Table 6.

Because of the lack of literature data for Pt-Ti interdiffusion, it is difficult to consider an interpretation of the experimental results, and therefore discussion of the results is not done at this time.

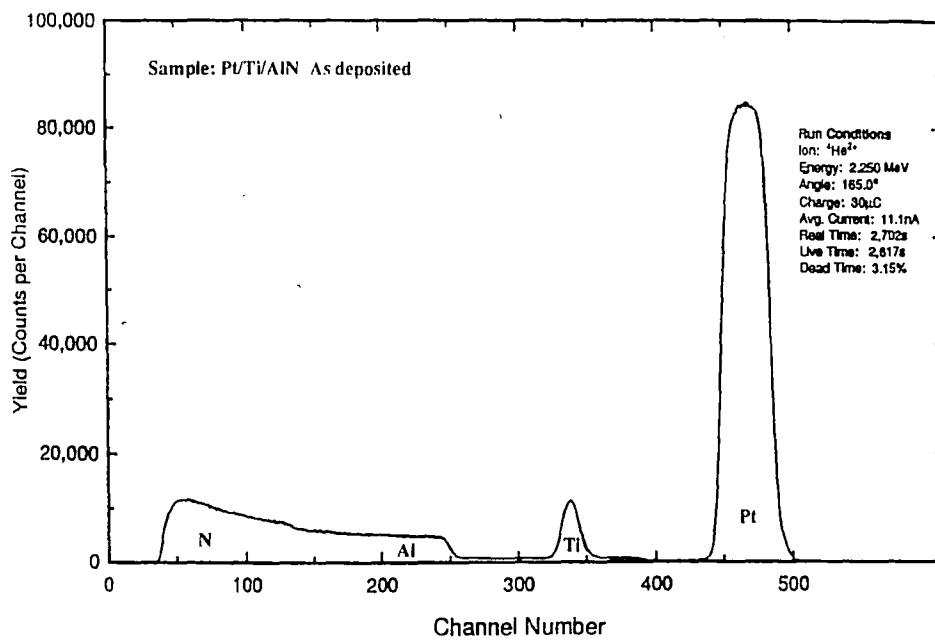


Figure 28 RBS spectrum of the as-deposited Pt/Ti/AlN specimen.

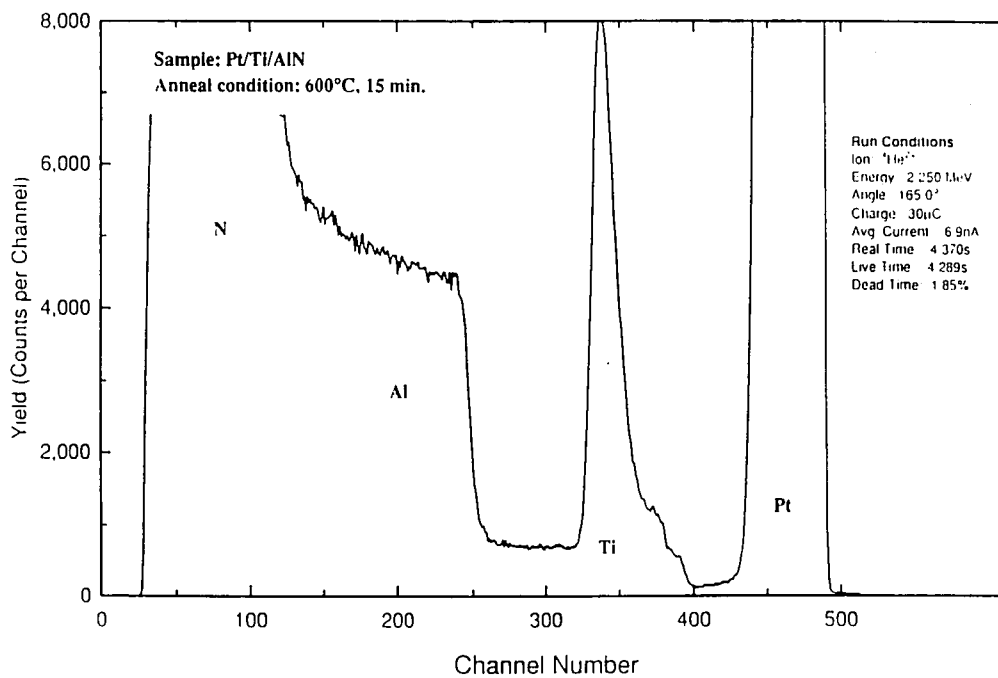


Figure 29 RBS spectrum of the Pt/Ti/AlN specimens annealed at 600°C for 15 min. in N₂ atmosphere.

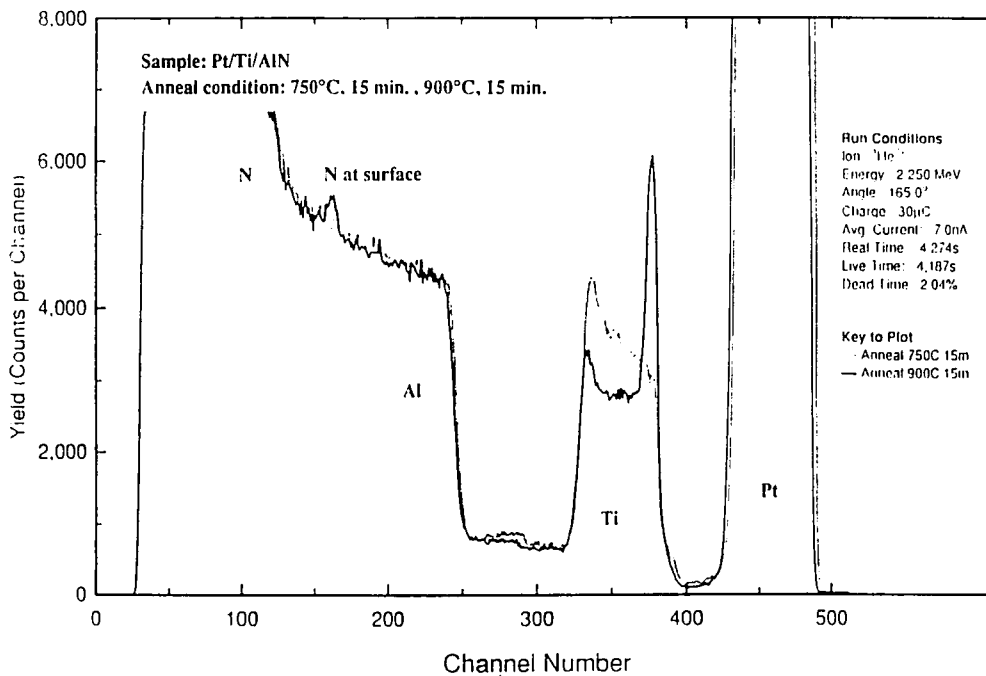


Figure 30 Superimposed RBS spectra of the Pt/Ti/AlN specimens annealed at 750°C and 900°C for 15 min. in N₂ atmosphere.

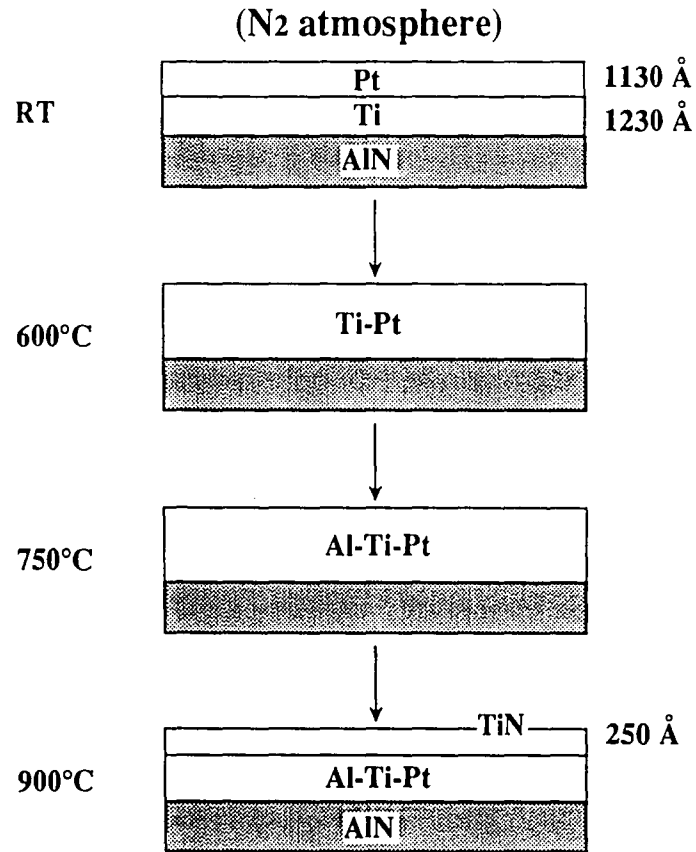


Figure 31 Schematic diagram of the reaction sequence between Pt/Ti/AlN annealed in N₂ atmosphere at different temperatures.

6. Conclusion

In order to clarify the fundamental knowledge regarding joining behavior and the adhesion mechanism for Ti and AlN, we studied the thin film reaction and diffusion of Ti/AlN, Ni/Ti/AlN and Pt/Ti/AlN, which are thin film combinations of industrial interest, using RBS. Moreover, the experimental results are interpreted in terms of thermodynamics and kinetics. As a result, we obtained the following conclusions.

- (1) Ni/Ti and Pt/Ti interdiffusion reactions are more rapid than reaction-diffusion in Ti/AlN. These results are in good agreement with literature diffusion data.
- (2) For the case of using a nitrogen atmosphere in the annealing process, TiN is formed on the top surface after Ti and either Ni or Pt are interdiffused. Ti reacts with ambient nitrogen.
- (3) Considering literature data for thermodynamic and kinetics behavior, when Ti/AlN is annealed in an Ar atmosphere, it is shown that TiN will be formed first at the interface between Ti/AlN and then TiAl₃ is formed.
- (4) To obtain interfacial reaction compounds such as TiN and TiAl₃, which make it possible to obtain high adhesion strength for Ti/AlN, a two step thin film deposition process is required in both Ni/Ti/AlN and Pt/Ti/AlN cases.

(5) Very preliminary results for the highest temperature diffusion (900°C) for Ni/Ti/AlN suggest the reaction products at the Ti/AlN interface to be TiN and Al (now dissolved in the Ni-Al layer).

(6) Rutherford Backscattering Spectrometry (RBS) is the effective method for examining the diffusion behavior of the thin film layers on AlN.

7. References

1. R. R. Tummala, E. J. Rymaszewski. *Microelectronics Packaging Handbook* : Van Nostrand Reinhold, 1989.
2. E. J. Rymaszewski, "Dense, Denser, Densest...", *J. Electronic Materials*, 18 [2] (1989): 217-220.
3. M. Pecht. *Handbook of Electronic Packaged Design*., Marcel Dekker Inc., 1991.
4. B. J. Landman, R. L. Russo, "Pin vs. Block Relationship for Partition of Logic Graphs.", *IEEE Trans. or Components*, C20(12) Dec. (1971): 1469-1479.
5. R. C. Chu, U. P. Huang, R. E. Simons, "Condition Cooling for an LSI Package: A one dimensional Approach.", *IBM J. Res. Develop.*, 26(1)Jan. (1982): 45-55.
6. K. Komeya, "Development of Nitrogen Ceramics", *Am. Ceram. Soc. Bull.*, 63[9] (1984): 1158-59, 1164.
7. N. Kuramoto, H. Taniguchi, I. Aso, "Translucent AlN Ceramic Substrate", *IEEE Transactions on Components, Hybrids and Manufacturing Technology*, Vol. CHMT-9, No. 4, Dec. (1986): 386-390.
8. D. A. Doane, P. D. Franzon, *Multichip Module Technologies and Alternatives*, Van Nostrand Reinhold, 1993.
9. S. Kimijima, T. Miyagi, T. Sudo, O. Shimada, "High-Density Multichip Module by Chip-on Wafer Technology.", *Proc. Int. Symp. Microelectron.* (1988) 314-319.

10. T. Inoue, H. Matsuyama, E. Matsuzaki, Y. Narizuka, M. Ishino, N. Tanaka, T. Takenaka, "Micro Carrier for LSI Chip used in the HITAC M-880 Processor Group." *Proc. 41st Electronic Components & Technology Conference*(1991): 704-711.
11. K. Niwa, Recent Progress in Ceramic Substrates Materials for Microelectronic Packaging", *Ceramic Transactions*, Vol. 33(1992): 115-124.
12. F. Miyashiro, N. Iwase, A. Tsuge, F. Ueno, M. Nakahashi, T. Takahashi, "High Thermal Conductivity Aluminum Nitride Ceramic Substrates and Packages.", *IEEE Transactions on Components, Hybrids and Manufacturing Technology*, Vol. CHMT-13, No. 2, June (1990): 313-319.
13. J. W. Balde, "Multichip Packaging and the Need for New Materials.", *J. Electronic Materials*, 18 [2] (1989) 221-227.
14. Y. Kurokawa, K. Utsumi, H. Takamizawa, T. Kamata, S. Noguchi, "AlN Substrates with High Thermal Conductivity.", *IEEE Transactions on Components, Hybrids and Manufacturing Technology*, Vol. CHMT-8, No. 2, June (1985): 247-252.
15. R. Chanchani, "Processability of Thin-Film, Fine-Line Pattern on Aluminum Nitride Substrates.", *IEEE Transactions on Components, Hybrids and Manufacturing Technology*, Vol. CHMT-11, No. 4, Dec. (1988): 427-432.
16. R. Chanchani, "Aluminum Nitride Substrates for Thin-Film Hybrid Integrated Circuits.", *Advances in Ceramics*, Vol. 26 (1989): 77-85.

17. A. Drost, D. Bonfert, M. Feil, "Reliability Investigations of Thin Film Metallizations on AlN-ceramics.", *Proceeding of IEEE/ISHM '90 IEMT Symposium-Italy*, 440-449.
18. K. J. Lodge, J. A. Sparrow, E. D. Perry, E. A. Logan, M. T. Goosey, D. J. Pedder, C. Montgomery, "Prototype Packages in Aluminum Nitride for High Performance Electronic Systems.", *IEEE Transactions on Components, Hybrids and Manufacturing Technology*, Vol. CHMT-13, No. 4, Dec. (1990): 633-638.
19. T. Yasumoto, K. Yamakawa, N. Iwase, N. Shinosawa, "Reaction between AlN and Metal Thin Films during High Temperature Annealing.", *J. the Ceramic Society of Japan*, 101[9](1993): 969-973.
20. Y. Kurokawa, H. Hamaguchi, Y. Shimada, K. Utsumi, H. Takamizawa, T. Kamata, S. Noguchi, "Development of Highly Thermal Conductive AlN Substrate by Green Sheet Technology.", *Proceeding 36th Electronic Components Conference (1986)*: 412-418.
21. M. Feil, W. Marder, "Investigation of Adhesion Mechanism of Ni-Cr Layers on Al₂O₃ and AlN Substrates.", *Proceeding 41st Electronic Components & Technology Conference (1991)*: 134-140.
22. T. Yasumoto, K. Yamakawa, N. Iwase, H. Asai, "The Mechanism of Aluminide Layer Growth between AlN Ceramics and Ti Thin Film during High Temperature Annealing.", *Proceeding of IUMRS (1993)*.

23. B. K. Brow, R. E. Loehman, A. P. Tomsia, J. A. Pask, "Interface Interactions During Brazing of AlN.", *Advances in Ceramics*, Vol. 26 (1989): 189-196.
24. B. K. Brow, R. E. Loehman, A. P. Tomsia, "Reactive metal Brazing of Aluminum Nitride.", *Metal-Ceramic Joining* (1991): 229-235.
25. R. E. Loehman, "Interfacial Reactions in Ceramic-Metal Systems.", *Ceram. Bull.*, 68[4](1989): 891-896.
26. R. E. Loehman, A. P. Tomsia, "Reactions of Ti and Zr with AlN and Al₂O₃.", *Acta metall. mater.*, Vol. 40, Suppl.(1992): S75-S83.
27. A. H. Carim, "Identification and Characterization of (Ti, Cu, Al)₆N, a New η Nitride Phase.", *J. Mater. Res.*, 4[6], Nov/Dec(1989): 1456-1461.
28. A. H. Carim, "High-Resolution Electron Microscopy of Interfaces in AlN-Braze Metal Alloy Systems.", *Mat. Res. Soc. Symp. Proc.*, Vol. 159(1990): 425-430.
29. A. H. Carim, R. E. Loehman, "Microstructure at the Interface between AlN and a Ag-Cu-Ti Braze Alloy.", *J. Mater. Res.*, 5[7], Jul(1990): 1520-1529.
30. M. Nakahashi, M. Shirokane, H. Takeda, "Characterization of Nitride Ceramic-Metal Joints Brazed with Ti Containing Alloys(in Japanese).", *J. Japan Inst. Metals*, 53[11](1989): 1153-1160.
31. T. Kuzumaki, T. Ariga, Y. Miyamoto, "Effect of Additional Elements in Ag-Cu Based Filler Metal on Brazing of Aluminum Nitride to Metals.", *ISIJ International*, 30[12](1990): 1135-1141.

32. Y. Kurihara, S. Takahashi, S. Ogihara, T. Kurosu, "Bonding Mechanism Between Aluminum Nitride Substrate and Ag-Cu-Ti Solder.", *IEEE Transactions on Components, Hybrids and Manufacturing Technology*, Vol. CHMT-15, No. 3, June (1992): 361-368.
33. M. G. Norton, J. M. Kajda, B. C. H. Steele, "Brazing of Aluminum Nitride Substrates.", *J. Mater. Res.*, 5[10], Oct(1990): 2172-2176.
34. M. G. Norton, J. M. Kajda, B. C. H. Steele, "A Technique for Brazing Aluminum Nitride Substrates.", *Mat. Res. Soc. Symp. Proc.*, Vol. 167(1990): 289-293.
35. M. G. Norton, "The Influence of Contact angle, Wettability, and Reactivity on the Development of Indirect-Bonded Metallizations for Aluminum Nitride.", *J. Adhesion Sci. Technol.*, 6[6](1992): 635-651.
36. J. C. Schuster, J. Bauer, "The Ternary System Titanium-Aluminum-Nitrogen.", *J. Solid State Chemistry*, 53, (1984): 260-265.
37. R. Beyers, R. Sinclair, M. E. Thomas, "Phase Equilibria in Thin-Film Metallizations.", *J. Vac. Sci. Technol.* B2(4), Oct.-Dec.(1984): 781-784.
38. A. D. Westwood, M. R. Notis, "AEM Study of Thin and Thick Film Metallization on AlN Substrates.", *Mat. Res. Soc. Symp. Proc.*, Vol. 108 (1988): 331-336.

39. A. D. Westwood, M. R. Notis, "Analytical Electron Microscopy Study of AlN Substrates and Metallization Interfaces.", *Advances in Ceramics*, Vol. 26 (1989): 171-187.
40. A. D. Westwood, M. R. Notis, "An issue in Thermal Management: Metallizing High Thermal Conductivity Ceramic Substrates in Microelectronics.", *JOM*, Jun. (1991): 10-15.
41. W. Chu, J. W. Mayer, M. A. Nicolet, *Backscattering Spectrometry*: Academic Press, 1978.
42. J. M. Poate, K. N. Tu, J. W. Mayer, *Thin films-Interdiffusion and Reactions*., John Wiley & Sons, 1978.
43. A. C. Miller, R. B. Irwin, H. F. Helbig, "Low-energy Ion Scattering and Rutherford Backscattering Spectroscopies.", *Physical Methods of Chemistry (Second edition)*, Vol. 9B, Interfaces(1993): 173-329.
44. W. K. Chu, G. Langouche, "Quantitative Rutherford Backscattering from Thin Films.", *MRS Bull.*, Jan.(1993): 32-40.
45. R. Kelly, C. Jech, H. Matzke, *Phys. stat. sol.*, 25, (1968): 641.
46. I. Barin, *Thermochemical Data of Pure Substances*, VCH, 1993.
47. J. Tardy, K. N. Tu, "Solute effect of Cu on interdiffusion in Al₃Ti compound films.", *Physical Review B*, 32[4], Aug.(1985): 2070-2081.
48. J. -P. Bars, D. David, E. Etchessahar, J. Debuigne, "Titanium a-Nitrogen Solid Solution Formed by High Temperature Nitriding: Diffusion of Nitrogen, Hardness, and Crystallographic Parameter.", *Metallurgical Transactions A*, 14A, Aug. (1983): 1537-1543.

49. A. Anttila, J. Raisanen, J. Keinonen, "Diffusion of Nitrogen in α -Ti.", *Appl. Phys. Lett.*, 42 [6] (1983): 498-500.
50. A. V. Pokoev, V. M. Mironov, L. K. Kudryavtseva, *Tsvetn. Metall.*, 2, (1976): 130-132.
51. J. Raisanen, A. Anttila, J. Keinonen, "Diffusion of Aluminum in Ion-implanted α -Ti.", *J. Appl. Phys.*, 57 [2] (1985): 613-614.
52. V. B. Rao, C. R. Houska, "Reactions and Diffusion between an Al Film and a Ti Substrate.", *Metallurgical Transactions A*, Vol. 14A, Jan. (1983): 61-66.
53. J. T. Klomp, "Physical aspects of ceramic-metal joining.", *Joining of Ceramics* ed. M. G. Nicholas, Chapman and Hall, 1993: 113-127.
54. G. F. Bastin, G. D. Rieck, "Diffusion in the Titanium-Nickel System: I. Occurrence and Growth of the various Intermetallic Compounds.", *Metallurgical Transactions*, 5, Aug. (1974): 1817-1826.
55. G. F. Bastin, G. D. Rieck, "Diffusion in the Titanium-Nickel System: II. Calculations of Chemical and Intrinsic Diffusion Coefficients.", *Metallurgical Transactions*, 5, Aug. (1974): 1827-1831.

8. Vita

Yoshihiko Imanaka was born to Eizaburo and Atsuko Imanaka on August 10, 1960, in Fukuoka city in Japan. In 1983 he graduated from Kyushu University with a BE in Metallurgical Engineering.

In that some year he joined Fujitsu Limited. Since then, he has performed research and developed multilayer ceramic circuit boards with copper conductors for super computer and mainframe computer applications. Prior to leaving for the United States, he was the research group leader for ceramic materials in the Microelectronics Packaging Laboratory at Fujitsu Laboratories Ltd.:

Just before arriving in the United States, he married Yoko Matsuo on July 11, 1992. He has been a graduate student in the Department of Material Science & Engineering at Lehigh University since the 1992 Fall semester, and has performed research under the guidance of Dr. Michael R. Notis.

He is a member of the Japanese Ceramic Society and the American Ceramic Society. He has six technical publications, excluding co-authored publications. He holds four US patents regarding ceramic circuit boards.

END

OF

TITLE